I&EC research
Industrial & Engineering Chemistry Research

Article

pubs.acs.org/IECR

Classical Density Functional Theory for Liquid–Fluid Interfaces and Confined Systems: A Functional for the Perturbed-Chain Polar Statistical Associating Fluid Theory Equation of State

Elmar Sauer and Joachim Gross*

Institute of Thermodynamics and Thermal Process Engineering, University of Stuttgart, Pfaffenwaldring 9, 70569 Stuttgart, Germany

Supporting Information

ABSTRACT: A Helmholtz energy functional based on the Perturbed-Chain Polar Statistical Associating Fluid Theory Equation of State is proposed. A weighted density approximation is used to develop two variants of dispersion functionals. We conduct molecular simulations (Monte Carlo) in order to assess both models. The structure of thin liquid adsorbed layers of a few molecular diameters thickness are shown to be particularly meaningful to detect deficiencies of Helmholtz energy functionals and thus discriminate between models. We further compare the model to experimental data of interfacial tensions for pure components and for binary mixtures exhibiting vapor−liquid equilibria and liquid−liquid equilibria. The proposed Helmholtz energy functional is in good agreement with experimental data of pure (organic) substances and mixtures and compares well with molecular simulation data of fluids adsorbing at solid interfaces.

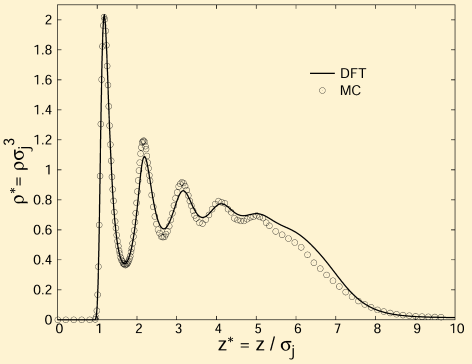

INTRODUCTION

Interfacial properties of vapor−liquid equilibria (VLE) and liquid−liquid equilibria (LLE), such as the interfacial tension, are essential for many technical applications. The study of solid−fluid interfaces is required to describe fluids in confinement (porous materials), and the predicted physical properties are for example adsorption isotherms, wetting phenomena, or the shift of phase equilibria due to confinement. As a unifying factor, all of these applications regard fluids as inhomogeneous systems, which means that the one-particle density varies in spacial coordinates. A powerful approach for the description of inhomogeneous liquid−fluid and solid−fluid interfaces is the classical density functional theory (DFT). A comprehensive discussion of the mathematical background of DFT is provided by Evans[1] and a compilation of possible applications is presented by Davis,[2] Löwen,[3] and Wu.[4]

The applied Helmholtz energy functional determines the accuracy of DFT predictions. Several types of approximations for the Helmholtz energy functional have been proposed, such as density expansion, integral equation theories, and perturbation approaches. A detailed overview is given in the reviews of Vanderlick et al.,[5] Evans,[6] Wu and Li,[7] and Emborsky et al.[8] Many DFT developments take a successful equation of state for bulk phases as a starting point and construct a suitable Helmholtz energy functional. In other cases, fluid theories are natively formulated in a functional form, as e.g., the first-order mean-spherical approximation of Tang and Wu.[9]

In several works, Helmholtz energy functionals have been developed by extending an expression of the Helmholtz energy initially developed for bulk phases. The simplest approach is the local density approximation (LDA), where the Helmholtz energy density $F[\rho(\mathbf{r})] = \int f[\rho(\mathbf{r})]\mathrm{d}\mathbf{r}$ of an inhomogeneous system with density profile $\rho(\mathbf{r})$ is calculated using the bulk phase Helmholtz energy density evaluated at the value of the local density, i.e., $f[\rho(\mathbf{r})] \approx f(\rho(\mathbf{r}))$. The round brackets indicate that f is a function of ρ whereas the square brackets define f as a functional. This approach is insufficient for most applications, especially if strongly oscillating density profiles occur and the values of local densities exceed the maximal packing fraction.

A significantly more successful approach is the weighted density approximation (WDA), where an appropriate bulk phase Helmholtz energy density is evaluated with a coarse grained or smoothed density. This so-called weighted density is obtained by averaging the one-particle density in defined regions and thus carries information on the inhomogeneity of the system. Note that the WDA is not limited to Helmholtz energy functionals, but has been used for other quantities such as direct correlation functions.[6]

A WDA can be applied to Helmholtz energy expressions for bulk phase properties. The family of Statistical Associating Fluid Theory (SAFT) models is a prominent and promising choice due to reliable results obtained from SAFT EoS for many applications. SAFT models are usually based on the first-order thermodynamic perturbation theory (TPT1) introduced by Wertheim.[10−13] After the first development of the SAFT

Received: November 23, 2016
Revised: March 14, 2017
Accepted: March 16, 2017
Published: March 17, 2017

ACS Publications

DOI: 10.1021/acs.iecr.6b04551
Ind. Eng. Chem. Res. 2017, 56, 4119−4135

framework,[14−17] several variants were proposed, such as soft-SAFT,[18,19] for potential of variable range (SAFT-VR),[20,21] Perturbed-Chain SAFT (PC-SAFT),[22,23] and SAFT-γ Mie.[24,25] We recommend the reviews of Müller and Gubbins,[26] Economou,[27] Paricaud et al.,[28] and Tan et al.[29] for a detailed study of SAFT. A review of how Wertheim developed the TPT is given in ref 30.

Wertheim's[10−13] perturbation theory has been applied to inhomogeneous systems by several groups. Kierlik and Rosinberg[31,32] presented a TPT1 functional and studied the behavior of polyatomic molecules in slit-shaped pores.[33] Segura and Chapman[34] performed Monte Carlo (MC) simulations of spherical molecules with four association sites confined near solid surfaces. They developed a model for determining monomer fractions (i.e., the fraction of molecules not associatively bonded) using Wertheim's theory and evaluated the theory using MC results. Segura et al.[35] presented and compared two methods for spherical associating molecules. The first method used an inhomogeneous form of Wertheim's theory whereas the second methods applied Tarazona's[36] weighted density to make the functional a simple extension of Wertheim's theory for bulk phases. A similar model has been applied to study the adsorption on surfaces with association sites.[37] Yu and Wu applied TPT1 to inhomogeneous systems and used the weighted densities of FMT[38−40] to develop functionals for associating interactions[41] and chain connectivity.[42] It has been applied successfully to confined systems and interfacial tensions.[43] Müller et al.[44] applied TPT1 to model Lennard-Jones chain molecules in inhomogeneous systems and used the WDA to formulate the Helmholtz energy functional. Their results show that the ranges of the WDA for the repulsive interactions and the WDA for attractive contributions are different.

A SAFT-variant applicable to inhomogeneous systems has been presented by Tripathi and Chapman[45,46] and is referred to as iSAFT. It models molecules as chains where the Helmholtz energy due to chain formation is developed from the association contribution in the limit of complete association and provides an accurate description of polymeric systems in confined media[45,46] and experimental surface tensions.[47] Jain et al.[48] modified iSAFT by ensuring that overall stoichiometry is satisfied by the density profiles and thus made iSAFT applicable to heteronuclear molecules. Subsequently, Bymaster and Chapman[49] extended the theory to model associating molecular chains.

In several works, SAFT EoS have been used as a basis in the development of DFTs. A DFT study of VLE interfaces was presented by Jackson and co-workers.[50,51] The proposed functional of the Helmholtz energy models the hard-sphere, chain, and association contributions at the LDA level whereas dispersive interactions are described as a mean-field approximation approach. In a subsequent study, Gloor et al.[52] developed and compared two additional Helmholtz energy functionals based on the SAFT-VR[20] EoS. The first functional describes the first-order dispersion term as a nonlocal perturbation theory and approximates the pair correlation function as a bulk phase radial distribution function. In the second variant, the first-order term is separated in a short-range contribution, approximated with the LDA, and a long-range contribution, where the pair correlation function is set to unity (mean field theory). Both functionals show good agreement with surface tensions of molecular simulations and experimental data. Gloor et al.[53] presented an approach, where experimental surface tensions are considered in the objective function of the adjustment of SAFT-VR pure component parameters.

The SAFT-FMT-DFT approach proposed by Schindler et al.[54] is also based on the SAFT-VR EoS. The chain contribution of the functional is based on the work of Yu and Wu.[42] The dispersion contribution is modeled via a second-order nonlocal perturbation theory where the pair correlation function is calculated using a weighted density of the FMT contribution. The functional is compared with results of MC simulations for confined systems defined by different external potentials. In subsequent work,[55] the functional was tested against experimental data of adsorption isotherms for several *n*-alkanes accounting also for the pore size distributions.

Malheiro et al.[56] presented and compared two additional functionals based on the SAFT-VR EoS for spherical components. Both approaches model the dispersion contribution of the Helmholtz energy functional via a WDA. The first approach uses the weighted densities obtained by the FMT term whereas the second approach uses a separately defined weighted density with Heaviside averaging. The second approach is superior and describes density profiles of confined systems very accurately. Subsequently,[57] the model extended by an association contribution according to Yu and Wu[41] and water was described in confined systems.

An EoS similarly to the SAFT-γ[24] EoS has been constructed by Ghobadi and Elliott[58] as a third-order Weeks−Chandler−Andersen[59] perturbation theory. Based on this EoS, a DFT framework has been developed that is applicable to confined systems and vapor−liquid interfaces.[60] Because of its group-contribution structure analogous to the SAFT-γ EoS, it is able to describe fused heteronuclear chains and it provides density profiles for all involved segment types. An extension of the DFT framework[61] to molecules with partial charges was established by including an association model according to Bymaster and Chapman.[49]

Several studies used the PC-SAFT EoS as a basis for constructing Helmholtz energy functionals. In previous work of our group,[62] we followed the work of Gloor et al.[52] and modeled the dispersion contribution as a nonlocal perturbation theory. To establish consistency with the PC-SAFT EoS a locally treated correction term was added. A comparison between a first- and a second-order dispersion functional showed nearly no difference in the calculation of surface tensions. The approach was extended to mixtures to describe interfacial tensions of vapor−liquid[63] and liquid−liquid phase equilibria.[64] A renormalization group theory was applied to ensure very good agreement in the vicinity of the critical point.[65] Von Müller and Leonhard applied the approach to surface tensions using PC-SAFT parameters obtained from quantum mechanical calculations.[66]

Shen et al.[67] presented a PC-SAFT-based Helmholtz energy functional referred to as hybrid PC-SAFT DFT. The dispersion contribution uses weighted densities proposed by Ye et al.,[68] where the density is averaged within a local sphere with radius 1.5σ. Density profiles in slit-shaped pores and adsorption isotherms were found in good agreement to results from molecular simulations and experimental data, respectively. Subsequently, an extension to mixtures and the influence of a WDA Lennard-Jonesian averaging were presented.[69] Also, pore size distributions were included into the model.[70]

In this work, two variants of a dispersion contributions to the Helmholtz energy functional are presented and compared. The superior variant is further evaluated by comparisons with experimental interfacial tensions and with density profiles obtained by MC simulations for solid–fluid interfaces.

■ CLASSICAL DENSITY FUNCTIONAL THEORY

The basic equation within DFT is the relation between the grand potential Ω and the intrinsic Helmholtz energy F, as[1,71]

$$\Omega[\rho_k] = F[\rho_k] + \sum_i^{N_c} \int \rho_i(\mathbf{r})\{V_i^{\text{ext}}(\mathbf{r}) - \mu_i\}\text{d}\mathbf{r} \tag{1}$$

where the density ρ_i of species i depends on the positional vector $\mathbf{r}$, and Ω and F are functionals of all densities ρ_k of the inhomogeneous system, and further N_c is the number of components. In this work, we use k as an generic index and $\rho_k(\mathbf{r})$ refers to the vector of all species–density profiles.

The integration is carried out over the volume V of the system. The external potential $V_i^{\text{ext}}(\mathbf{r})$ describes interactions between a molecule of component i at position $\mathbf{r}$ and an external field. For a system with given temperature T, volume V and chemical potentials μ_i, thermodynamic equilibrium requires Ω to be minimal with respect to all internal degrees of freedom, such as the density profiles $\rho_k(\mathbf{r})$. In fact, it is appropriate to speak of Ω as the grand potential only in its minimized state with respect to internal degrees of freedom, i.e., the density profiles $\rho_k(\mathbf{r})$ in our case. The first functional derivative of Ω with respect to the ρ_j is thus zero for all components j

$$\frac{\delta\Omega[\rho_k]}{\delta\rho_j(\mathbf{r}^*)} = 0 \tag{2}$$

The equilibrium condition applied to eq 1 leads to

$$0 = \frac{\delta F[\rho_k]}{\delta\rho_j(\mathbf{r}^*)} + V_j^{\text{ext}}(\mathbf{r}^*) - \mu_j^{\text{b}} \tag{3}$$

All inhomogeneous systems shown in this work are connected to bulk phases (superscript b). Because when thermodynamic equilibrium prevails, the chemical potentials are uniform over space and therefore $\mu_j = \mu_j^{\text{b}}$. Separating F and μ_j^{b} into an ideal gas (id) and a residual (res) contribution leads to

$$\rho_j(\mathbf{r}^*) = \rho_j^{\text{b}}\exp\left[\frac{\mu_j^{\text{res,b}}}{kT} - \frac{\delta\frac{F^{\text{res}}[\rho_k]}{kT}}{\delta\rho_j(\mathbf{r}^*)} - \frac{V_j^{\text{ext}}(\mathbf{r}^*)}{kT}\right] \tag{4}$$

where k is Boltzmann's constant. In eq 4, we canceled the de Broglie wavelength Λ_i from the functional derivative of the ideal gas Helmholtz energy

$$F^{\text{id}}[\rho_k] = kT\sum_i^{N_c}\int \rho_i(\mathbf{r})\{\ln(\rho_i(\mathbf{r})\Lambda_i^3) - 1\}\text{d}\mathbf{r} \tag{5}$$

and from the ideal gas chemical potential

$$\mu_j^{\text{id,b}} = kT\ln(\rho_j^{\text{b}}\Lambda_j^3) \tag{6}$$

Ideal gas here refers to molecular species in a state where intermolecular interactions do not exist. The connectivity of segments to form chains (molecules) is considered using Wertheim's perturbation theory[10−13] within the chain term, described below. Details are given in Appendix D.

Application: Interfacial Tensions. We briefly summarize how the surface tension between vapor and liquid phases (VLE) of mixtures as well as the interfacial tension of two liquid phases (LLE) were calculated in this work. A more comprehensive description of the general calculation procedure is given by Klink and Gross.[63] For given temperature T (pure components) or given temperature T and pressure p (binary mixtures), the phase equilibrium is determined with the PCP-SAFT EoS. The phase equilibrium calculation delivers the required bulk chemical potentials $\mu_j^{\text{res,b}}$ as well as bulk densities ρ_j^{b} for both coexisting phases. We consider planar interfaces using a cylindrical coordinate system, with z-coordinate normal to the interface. The density varies only along the z-coordinate, and one can perform simple one-dimensional DFT calculations for the interfacial tensions.

Equation 4 is solved iteratively using a damped direct substitution scheme (Picard iteration). The starting profile of the partial densities are generated using a hyperbolic tangent function proposed by Klink et al.[64]

$$\rho_j^{(0)}(z) = \frac{1}{2}(\rho_j^{\text{b,P1}} + \rho_j^{\text{b,P2}}) + \frac{1}{2}(\rho_j^{\text{b,P1}} - \rho_j^{\text{b,P2}})\tanh\left(0.6\frac{z}{\sigma_j}\right) \tag{7}$$

where the coexisting phases are denoted by P1 and P2 and σ_j is the PCP-SAFT segment size parameter.

For converged density profiles defining the equilibrium state, the interfacial tension can be calculated using

$$\gamma = \int\left(f[\rho_k(z)] - \sum_i^{N_c}\mu_i\rho_i(z) + p^{\text{b}}\right)\text{d}z \tag{8}$$

with p^{b} as the scalar valued pressure of bulk phases in phase equilibrium, which is equal to the normal pressure for planar interfaces. The Helmholtz energy density $f[\rho_k(z)]$ is defined by

$$F[\rho_k] = A\int f[\rho_k(z)]\text{d}z \tag{9}$$

where A is the area of the considered planar interface.

Application: Confined Systems. The DFT is a powerful framework also for studying the behavior of fluids in confinement. We assume solid walls, which determine the geometry of the confinement, to be perfectly plain (without roughness) and chemically homogeneous. We focus on graphite-like slit-shaped pores. With these assumptions, density profiles vary only along the z-coordinate, where the z-axis points perpendicular to the planar wall. The same one-dimensional implementation used for the calculation of interfacial tensions can be used for these slit-shaped pores.

The intermolecular interactions within the fluid phase is covered by the intrinsic Helmholtz energy, whereas molecular solid–fluid interactions are described through the external potential V_j^{ext} acting on fluid molecules of species j. For the external potential, in this work we use the 9,3 potential

$$V_{js}^{\text{ext}}(z) = \varepsilon_{js}\left[\left(\frac{\sigma_{js}}{z}\right)^9 - \left(\frac{\sigma_{js}}{z}\right)^3\right] \tag{10}$$

where the subscripts j and s denote the fluid component and the solid species, respectively. Binary solid–fluid interaction parameters are defined by the Berthelot–Lorentz combining rules $\sigma_{js} = \frac{1}{2}(\sigma_{jj} + \sigma_{ss})$ and $\varepsilon_{js} = \sqrt{\varepsilon_{jj}\varepsilon_{ss}}$, where ε denotes dispersive energy parameters. Furthermore, we apply the frequently used external 10,4,3 potential proposed by Steele,[72] as

$$V_{js}^{\mathrm{ext}}(z) = 2\pi\rho_s\varepsilon_{js}\sigma_{js}^2\Delta\left[\frac{2}{5}\left(\frac{\sigma_{js}}{z}\right)^{10} - \left(\frac{\sigma_{js}}{z}\right)^{4} - \frac{\sigma_{js}^4}{3\Delta(z+0.61\Delta)^3}\right] \tag{11}$$

The solid phase is thereby described as a stack of lattice planes, assumed as idealized basal graphite planes. The distance between lattice planes is defined by distance parameter Δ and the overall density of the solid phase is ρ_s. Interactions of the fluid molecules with the topmost lattice plane (adjacent to the fluid phase) leads to the first and second term on the right-hand side of eq 11. The subjacent lattice planes interact with the fluid molecules according to the third term. The z-coordinate is defined as the distance between the center of a solid particle on the topmost lattice plane and the center of a fluid molecule. A parameter set[72,73] for a graphite solid phase is given: σ_{ss} = 3.40 Å, ε_{ss}/k = 28.0 K, Δ = 3.35 Å, and ρ_s = 0.114 Å^{-3}.

The external field acting on a molecule of type j at position z resulting from the solid-phase on both sides of the slit-shaped pore is obtained by superposition

$$V_j^{\mathrm{ext}}(z) = V_{js}^{\mathrm{ext}}(z) + V_{js}^{\mathrm{ext}}(H-z) \tag{12}$$

where H is the distance between the centers of the topmost wall particles of both planar walls. $V_{js}^{\mathrm{ext}}(z)$ describes the interaction of a fluid molecule with the solid phase on the left side and $V_{js}^{\mathrm{ext}}(H-z)$ with the solid phase on the right side.

The grand potential Ω is minimal with respect to the equilibrium density profiles $\rho_k(\mathbf{r})$ for defined variables T, V, and μ_k. We choose the input variables by (hypothetically) connecting the inhomogeneous system to a bulk phase system. The natural variables are then given as thermodynamic equilibrium conditions of the connected bulk phase, $T = T^{\mathrm{b}}$ and $\mu_i = \mu_i^{\mathrm{b}}$. The temperature T^{b} (and volume V) of the considered system are usually easy to define, whereas the chemical potentials need to be determined from the EoS by considering the bulk phase system at given (T, p).

■ HELMHOLTZ ENERGY FUNCTIONAL

The Helmholtz energy functional entirely determines the quality of DFT predictions. In this section, we propose a new Helmholtz energy functional that is consistent with the PCP-SAFT EoS. More specifically, we present a new functional term for the dispersive (attractive) interactions, which is suitable for both, confined systems and for VLE or LLE interfaces. At the same time, the new functional can be solved very efficiently compared to our previous work.[62,63]

In accordance with the structure of the PCP-SAFT EoS, we consider a functional composed of several contributions

$$F^{\mathrm{res}}[\rho_k] = F^{\mathrm{hs}}[\rho_k] + F^{\mathrm{hc}}[\rho_k] + F^{\mathrm{disp}}[\rho_k] + F^{\mathrm{assoc}}[\rho_k] + F^{\mathrm{mp}}[\rho_k] \tag{13}$$

where the superscripts (hs, hc, disp, assoc, and mp) denote hard-sphere, chain, dispersion, association, and multipolar contributions, respectively. To provide a DFT that is consistent with the PCP-SAFT EoS, it is required that all contributions of eq 13 simplify to the corresponding contributions[23,74−77] of the reduced Helmholtz energy $\tilde{a} = F/NkT$ for homogeneous phases, with N as the total number of molecules in the system. This section is focused on the proposed dispersion contribution, but a short description of all contributions in eq 13 is given.

The Hard-Sphere Contribution. The fundamental measure theory (FMT) originally proposed by Rosenfeld[38] and simultaneously modified by Roth et al.[39] and Yu and Wu[40] very accurately describes the behavior of inhomogeneous hard-sphere systems. The bulk EoS that corresponds to the modified FMT[39,40] is the hard-sphere EoS proposed by Mansoori et al.[78] The modified FMT is thus consistent with the PCP-SAFT hard-sphere contribution. In the appendix of previous work,[62] we formulated the modified FMT integrals for one-dimensional cylindrical coordinate systems, where the density profile depends only on the z-coordinate. Unfortunately, we presented an erroneous equation and discuss the correction of the error in Appendix A.

The Chain Contribution. The chain contribution to the Helmholtz functional used in this work has been developed by Tripathi and Chapman[45,46] and is based on Wertheim's first-order perturbation theory.[10−13] The here considered version of PCP-SAFT EoS regards nonspherical molecules as chains of equal spherical segments (homonuclear chains). The corresponding chain functional reads

$$\frac{F^{\mathrm{hc}}[\rho_k]}{kT} = \sum_i (m_i - 1)\int \rho_i(\mathbf{r})(\ln\rho_i(\mathbf{r}) - 1)\mathrm{d}\mathbf{r} - \sum_i (m_i - 1)\int \rho_i(\mathbf{r})(\ln[y_{ii}^{\mathrm{dd}}(\bar{\rho}_k^{\mathrm{hc}}(\mathbf{r}))\lambda_i(\mathbf{r})] - 1)\mathrm{d}\mathbf{r} \tag{14}$$

The ideal gas reference state used by Tripathi and Chapman[46] (and natively obtained from Wertheim's theory) is the ideal gas state of nonbonded segments. The chain functional in eq 14 differs from the chain functional of Tripathi and Chapman[46] because the ideal gas reference state used in the PCP-SAFT formalism is defined for complete molecules. The difference between both functionals ensures the consistency with the chain contribution of the PCP-SAFT EoS. For further details, see Appendix D.

In the derivation of eq 14, ρ_i is an average of density profiles of segments in molecule i. Therefore, eq 14 does not provide density profiles of individual segments in a molecule. For some cases, like for surfactants, a distinction between density profiles of individual segments is an interesting perspective. An extension of the theory to heteronuclear molecules is described in the work of Jain et al.[48] This DFT concept is appealing for heteronuclear chains, used for example in group-contribution methods.[79]

The Contribution from Dispersive Attractions. A dispersive term compatible with the PCP-SAFT EoS has been proposed in earlier work.[62,63] This earlier term has strengths in the accuracy of predictions, that are possible for interfacial tensions of pure substances and mixtures. At the same time, there are disadvantages, namely the functional is not suited for interfaces to solids, where significant local fluctuations of the single-particle density occur. Second, the term is rather involved, both in implementation and in computational cost. We here strive to alleviate these deficiencies with a new term that is suitable for systems with confining solid−fluid interfaces while at the same time maintaining the accuracy of our earlier functional term. In this section, the structure of an alternative contribution $F^{\mathrm{disp}}[\rho_k]$ is suggested. A discussion of benefits and disadvantages of the former and the new dispersion contribution as well as a comparison between them is given in the Results and Discussion section.

Definition of Weighted Densities for Dispersion of PCP-SAFT EoS. For the weighted densities, we adopt the formulation proposed by Tarazona[80,81]

$$\bar{\rho}_i(\mathbf{r}_1) = \int \rho_i(\mathbf{r}_2) w_i(|\mathbf{r}_1 - \mathbf{r}_2|) \mathrm{d}\mathbf{r}_2 \tag{15}$$

where $\bar{\rho}_i$ is the weighted density of component i for position $\mathbf{r}_1$ and w_i is the corresponding normalized weighting function. In several works,[36,82,83] a density dependent weighting function has been proposed. Our aim is to keep the dispersion contribution as simple as possible and therefore no density dependence is introduced. We define the normalized weighting function of component i as

$$w_i(r) = \frac{\Theta[\psi d_i - r]}{\int \Theta[\psi d_i - |\mathbf{r}_3|] \mathrm{d}\mathbf{r}_3} \tag{16}$$

with d_i as the temperature dependent effective repulsive (hard-sphere) diameter and Θ as the Heaviside function. We summarize the basis to the weighted density approach in Appendix C and reveal the involved assumptions. The appendix shows that other weight functions are possible (and are in fact more obvious than a Heaviside-weight); however, we value the simplicity of the Heaviside function, particularly because Heaviside-weighted densities are already required for the Fundamental Measure Theory. That choice ensures a simple implementation and high computational efficiency. In Appendix C, we discuss other choices, such as a weight according to the attractive part of the Lennard-Jones potential or a square-well potential and we mention that the considered alternative choices gave no advantage for our applications. We introduced the parameter ψ, which scales the size of the averaging space, analogously to Ye et al.[68] Instead of defining ψ = 1.5, we interpret ψ as an universal but (one time) adjustable model parameter. Because of the long-ranged nature of dispersive interactions, it is sensible to assume that ψ values are larger than 1. With the weighting function, the weighted density used in this work is

$$\bar{\rho}_i(\mathbf{r}_1) = \frac{3}{4\pi\psi^3 d_i^3} \int \rho_i(\mathbf{r}_2) \Theta[\psi d_i - |\mathbf{r}_1 - \mathbf{r}_2|] \mathrm{d}\mathbf{r}_2 \tag{17}$$

Structure of the New Dispersion Contribution. The basic idea behind WDA is to cast a model valid for homogeneous systems into functional form, applicable to inhomogeneous systems. In our case, the reduced dispersion contribution to the Helmholtz energy $\tilde{a}^{\mathrm{disp}}$ has to be written in functional form. We suggest two simple and straightforward variants of the functional, noting that several more variants are conceivable. In variant WDA1, the full Helmholtz energy density is modeled via weighted densities so that

$$\frac{F^{\mathrm{disp},1}[\rho_k]}{kT} = \int \bar{\rho}(\mathbf{r}_1) \tilde{a}^{\mathrm{disp}}(\bar{\rho}_k(\mathbf{r}_1)) \mathrm{d}\mathbf{r}_1 \quad \text{(WDA1)} \tag{18}$$

where $\tilde{a}^{\mathrm{disp}}$ is a function of all weighted densities at position $\mathbf{r}_1$ and $\bar{\rho}$ is the locally defined total weighted density

$$\bar{\rho}(\mathbf{r}_1) = \sum_j \bar{\rho}_j(\mathbf{r}_1) \tag{19}$$

For variant WDA2, $\tilde{a}^{\mathrm{disp}}$ is multiplied by the local value of the density ρ instead of $\bar{\rho}$, which leads to

$$\frac{F^{\mathrm{disp},2}[\rho_k]}{kT} = \int \rho(\mathbf{r}_1) \tilde{a}^{\mathrm{disp}}(\bar{\rho}_k(\mathbf{r}_1)) \mathrm{d}\mathbf{r}_1 \quad \text{(WDA2)} \tag{20}$$

WDA models in form of eq 20 are dominant in the literature. Earlier studies with strongly oscillating density profiles showed that, in combination with eq 16, the influence of the local density $\rho(\mathbf{r}_1)$ in eq 20 leads to insufficient results. As a result, eq 18 has been introduced as an alternative model, where the direct influence of $\rho(\mathbf{r}_1)$ is reduced. An approach similar to eq 18 was proposed also by Peng and Yu.[84,85]

The formulation of variant WDA2 is closely related to the approach presented by Shen et al.[69] Their model is for pure component systems equal to eq 20 but both models differ slightly for mixtures. Note, the similarity of both approaches concern the structure of eq 20. But we will use a different definition for the weighted densities, compared to Shen et al. so that results for pure components from both approaches differ in any practical calculation. A comparison with the Shen et al. functional is shown in Appendix B. Note that two additional WDA approaches have been derived that were discarded due to insufficient accuracy in confined systems. The derivation and discussion is presented in Appendix C.

The evaluation of $\tilde{a}^{\mathrm{disp}}$ with weighted densities is

$$\tilde{a}^{\mathrm{disp}}(\bar{\rho}_k(\mathbf{r}_1)) = -2\pi\bar{\rho}(\mathbf{r}_1) I_1(\bar{\eta}, \bar{m}) \overline{m^2\varepsilon\sigma^3} - \pi\bar{\rho}(\mathbf{r}_1)\bar{m} C_1 \times I_2(\bar{\eta}, \bar{m}) \overline{m^2\varepsilon^2\sigma^3} \tag{21}$$

with the mean segment number

$$\bar{m} = \sum_i \bar{x}_i m_i \tag{22}$$

where m_i is the PC-SAFT segment number. The abbreviations $\overline{m^2\varepsilon\sigma^3}$, $\overline{m^2\varepsilon^2\sigma^3}$ and C_1 calculate as[23]

$$\overline{m^2\varepsilon^n\sigma^3} = \sum_i \sum_j \bar{x}_i \bar{x}_j m_i m_j \left(\frac{\varepsilon_{ij}}{kT}\right)^n \sigma_{ij}^3 \tag{23}$$

and

$$C_1 = \left[1 + \bar{m}\frac{8\bar{\eta} - 2\bar{\eta}^2}{(1-\bar{\eta})^4} + (1-\bar{m})\frac{20\bar{\eta} - 27\bar{\eta}^2 + 12\bar{\eta}^3 - 2\bar{\eta}^4}{[(1-\bar{\eta})(2-\bar{\eta})]^2}\right]^{-1} \tag{24}$$

The packing fraction $\bar{\eta}$ and the mole fraction $\bar{x}_i$ are locally defined as

$$\bar{\eta} = \frac{\pi}{6}\sum_i \bar{\rho}_i(\mathbf{r}_1) m_i d_i^3 \tag{25}$$

$$\bar{x}_i = \frac{\bar{\rho}_i(\mathbf{r}_1)}{\bar{\rho}(\mathbf{r}_1)} \tag{26}$$

The parameters σ_{ij} and ε_{ij} are defined by Lorentz–Berthelot combining rules using PC-SAFT segment diameters σ_{ii} and PC-SAFT potential depth ε_{ii}, respectively.

Evaluation of WDA Variants. In the previous paragraph, we presented two dispersion functionals. We treat ψ for both variants as (one time) adjustable and subsequently universal model constant and evaluate whether the dispersion functional maintains its predictive qualities for a variety of applications. We adjusted the values of the ψ parameters for both variants by minimizing the root-mean-square (%RMS) deviations of calculated surface tensions from experimental values. We thereby considered 168 data points for the surface tension, referred to as experimental data points, in the DIPPR database,[86] of *n*-alkanes (methane, ethane, propane, butane, hexane, heptane, octane, tridecane, pentadecane, hexadecane, and octadecane). Because of the known overestimation of critical points by the PCP-SAFT EoS, we omitted experimental data points at temperatures above $0.95 \cdot T_c$, where T_c is the critical temperature of the considered substance. The calculated surface tensions were obtained according to the procedure described above. PCP-SAFT pure component parameters were taken from Gross and Sadowski[23] and are listed as Supporting Information.

Both variants show a similar accuracy in the correlation of the experimental data. The %RMS (%AAD) values obtained are 4.24% (2.63%) and 4.01% (2.06%) for WDA1 and WDA2, respectively. The performance of both WDA variants is comparable; however, WDA2 is slightly better for surface tensions of *n*-alkanes. The optimized values of the parameters are $\psi_{\mathrm{WDA1}} = 1.3862$ and $\psi_{\mathrm{WDA2}} = 1.8738$. We studied whether ψ depends on the segment number m_i and have not found strong segment number dependence. A graphical description of the adjustment results are shown in the Results and Discussion section.

The Associative Attraction. In previous work on interfacial tensions of liquid−liquid equilibria, we adopted the LDA for the association term.[64] The density profile in such systems is rather smooth, as opposed to solid−fluid interfaces, so that we assumed the LDA to be sufficient for the association term. In the meantime, we came to the conclusion that the LDA is not adequate, even for fluid interfaces. For solid−fluid interfaces, deficiencies of the LDA are amplified. We now describe the association contribution to the Helmholtz functional with the WDA functional presented by Yu and Wu.[41] An advantage of this functional is that within a DFT calculation no further weighted densities need to be calculated because it is based on scalar as well as vector-weighted densities defined by the FMT.

With some generalizations and minor modifications to the functional presented by Yu and Wu,[41] based on Wertheim's TPT[10−13] and the extension of Chapman et al.[15] we obtain a functional consistent with the PCP-SAFT association contribution. The associative Helmholtz energy functional is

$$F^{\mathrm{assoc}}[\rho_k] = \int f^{\mathrm{assoc}}[\rho_k]\mathrm{d}\mathbf{r} \tag{27}$$

with the associative Helmholtz energy density

$$f^{\mathrm{assoc}}[\rho_k] = kT \sum_i \frac{n_{0i}}{m_i}\xi_i \sum_{A_i}^{\{A_i\}} N_{A_i}\left(\ln \chi^{A_i}(\mathbf{r}) - \frac{\chi^{A_i}(\mathbf{r})}{2} + \frac{1}{2}\right) \tag{28}$$

where the outer sum runs over all components and the inner sum runs over all types of association sites A_i of species *i*. Further, N_{A_i} is the number of association sites of type A_i and $\chi^{A_i}(\mathbf{r})$ is the locally defined monomer-fraction of type A_i (i.e., fraction of nonbonded association sites), calculated as

$$\chi^{A_i}(\mathbf{r}) = \left[1 + \sum_j \frac{n_{0j}}{m_j}\xi_j \sum_{B_j} N_{B_j}\chi^{B_j}(\mathbf{r})\Delta^{A_iB_j}(\mathbf{r})\right]^{-1} \tag{29}$$

with $\Delta^{A_iB_j}(\mathbf{r})$ as the locally defined association strength between association sites A_i and B_j

$$\Delta^{A_iB_j}(\mathbf{r}) = \sigma_{ij}^3\kappa^{A_iB_j}\left[\exp\left(\frac{\varepsilon^{A_iB_j}}{kT}\right) - 1\right]g_{ij}^{\mathrm{hs}}(n_\alpha) \tag{30}$$

with $\kappa^{A_iB_j}$ and $\varepsilon^{A_iB_j}$ as the adjustable association parameters. The radial distribution function of hard-spheres is given as

$$g_{ij}^{\mathrm{hs}}(n_\alpha) = \frac{1}{1 - n_3} + d_{ij}\frac{n_2\xi}{2(1 - n_3)^2} + d_{ij}^2\frac{n_2^2\xi}{18(1 - n_3)^3} \tag{31}$$

The factors ξ and ξ_i as well as the component-wise weighted densities $n_{\alpha i}$ are defined according to Yu and Wu[41]

$$\xi = 1 - \frac{\mathbf{n}_{V2}\cdot\mathbf{n}_{V2}}{n_2^2} \tag{32}$$

$$\xi_i = 1 - \frac{\mathbf{n}_{V2i}\cdot\mathbf{n}_{V2i}}{n_{2i}^2} \tag{33}$$

$$n_{\alpha i} = n_{\alpha i}(\mathbf{r}) = m_i \int \rho_i(\mathbf{r}')w_{\alpha i}^{\mathrm{FMT}}(\mathbf{r} - \mathbf{r}')\mathrm{d}\mathbf{r}' \quad \text{with } \alpha = \{0, 2, 3, V2\} \tag{34}$$

where $w_{\alpha i}^{\mathrm{FMT}}$ are weights defined by the FMT.[38] The overall weighted densities $n_\alpha = \sum_i n_{\alpha i}$ are the same weighted densities used in the FMT functionals.[38−40,87]

The Multipolar Attraction. Multipolar interactions between molecules are taken into account using the weighted densities defined above, with

$$\frac{F^{\mathrm{mp}}[\rho_k]}{kT} = \int \bar{\rho}(\mathbf{r})\tilde{a}^{\mathrm{mp}}(\bar{\rho}_k(\mathbf{r}))\mathrm{d}\mathbf{r} \tag{35}$$

where $\tilde{a}^{\mathrm{mp}}$ is the sum of the bulk phase dipole−dipole,[76] dipole−quadrupole,[75] and quadrupole−quadrupole[77] contribution.

■ RESULTS AND DISCUSSION

The objective of this work is to propose a simple Helmholtz energy functional that can be used to predict interfacial tensions as well as density profiles of fluids in confined systems. In this section, the two variants of the dispersion contribution presented above are compared to experimental data and to results from molecular simulations. A model constant ψ, adjusted to vapor−liquid surface tensions of *n*-alkanes, has gone into both variants of the Helmholtz energy functional. First, we compare results of both variants to the density profile for liquid (adsorbed) film on a solid wall obtained by MC simulations. This case allows us to discriminate clearly between both models and choose the superior variant. Subsequently, we demonstrate the transferability of the so-obtained functional to confined systems. Finally, we assess predictions of the models for interfacial tensions of pure components and mixtures, in comparison to experimental data. Also, a comparison between the suggested functional of this work, F^{disp}, to results from our earlier work[62−64] is provided. We note, the focus of this work is on evaluating the dispersion functional. Substances with strong associative (hydrogen bonding) or polar interactions are not considered.

We use experimental data for the validation of interfacial tensions. Experimental data for assessing the theory for confined systems would also be desirable. Experimental adsorption isotherms, for example, should be appropriate in this context. A meaningful comparison between DFT and experimental adsorption isotherm data, however, necessitates

DOI: 10.1021/acs.iecr.6b04551
Ind. Eng. Chem. Res. 2017, 56, 4119−4135

detailed knowledge of the solid surface. The solid would need to be characterized in the geometrical shape of pores, the pore size distribution, and the (effective) solid−fluid interaction.[88] This detail is not available for typical porous materials and we thus compare density profiles from DFT calculations with density profiles obtained from MC simulations, where we have full control over pore-shape and solid−fluid interaction potentials.

Liquid Film on Solid Wall. As a first application of the DFT with the WDA dispersion functional to solid−fluid interfaces, we regard a pure component density profile of a Lennard-Jones fluid with the parameters σ_{jj} and ε_{jj}. We performed a MC simulation in the grand-canonical ensemble to obtain the density profile. The 9,3 potential, eq 10, is used as an external potential with the parameters $\sigma_{js} = \sigma_{jj}$ and $\varepsilon_{js} = 8\ \varepsilon_{jj}$. A relatively high value for ε_{js} leads to strong attractive interaction between solid and fluid molecules. Although the behavior of a fluid component next to a single wall is of interest, a MC simulation within a slit-shaped pore geometry, eq 12, is carried out. The distance between both pore walls is chosen sufficient far, $H = 35\ \sigma_{jj}$, to prevent interactions between particles of the liquid film of one side of the simulation box with particles of the film of the other side of the box. The system size is chosen to be 30 σ_{jj} in spatial direction parallel to the solid wall. The cutoff radius is set to the high value of $r_c = 15\ \sigma_{jj}$, avoiding the need for cutoff corrections. This cutoff value does not limit interactions in the *z*-direction, normal to the interface, so that the cutoff is active in two of the three dimensions of the system. The dimensionless temperature is set to $T^* = T\frac{k}{\varepsilon_{\mathrm{jj}}} = 0.9$, and for the excess chemical potential we defined $\mu_j^* = \frac{\mu_j}{\mathrm{kT}} - 3\ln\left(\frac{\Lambda_j}{\text{Å}}\right) = -4.45$. The number of particles in the system varies during the simulation between 7000 and 8700. For sampling the single-particle density profile $\rho(z)$, we divided the normal coordinate in 1750 slabs of equal width Δz.

The PCP-SAFT model is not a true Lennard-Jones equation of state. The properties of a Lennard-Jones fluid are in practice, however, described very well. A comparison between PC-SAFT and the LJ EoS presented by Johnson et al.[89] with $0.5\ T_c < T^* < 0.9\ T_c$ yields deviations of 1.20% and 2.65% in vapor pressure and liquid density, respectively. We thereby use the PC-SAFT parameters as Lennard-Jones parameters, with $m_i = 1$. DFT calculations are performed for both variants of the Helmholtz energy functional for the dispersion contribution.

The resulting density profiles of the liquid film are shown in Figure 1. The MC simulation gives a liquid film with a film thickness of approximately 7 σ_{jj}. A comparison between the WDA1 and the WDA2 variant shows a clear advantage of the WDA1 model. In contrast to WDA2, the WDA1 variant predicts the z^* position of density peaks and valleys in good agreement to the simulation data. The WDA1 model also captures the amplitude of density oscillations much better than the WDA2 model. Furthermore, the WDA2 variant does not provide a smooth description of the density undulations along the z^* coordinate, as can be seen in the range $z^* = 2.7$−3.3. Both models somewhat overestimate the density profile in the range $z^* = 5$−8. The overall agreement of the WDA1 model to data from MC simulations, however, is very good.

We chose the WDA1 model as our preferred model of the dispersion contribution, due to the better behavior in Figure 1. We find the adsorbed (liquid-like) film regarded in Figure 1 discriminates between different Helmholtz energy functionals in a very sensitive manner, whereas interfacial tensions of pure components were not allowing a meaningful discrimination of models (noting that a model constant ψ was adjusted to pure component interfacial tensions). The WDA1 model will henceforth be referred to as DFT model.

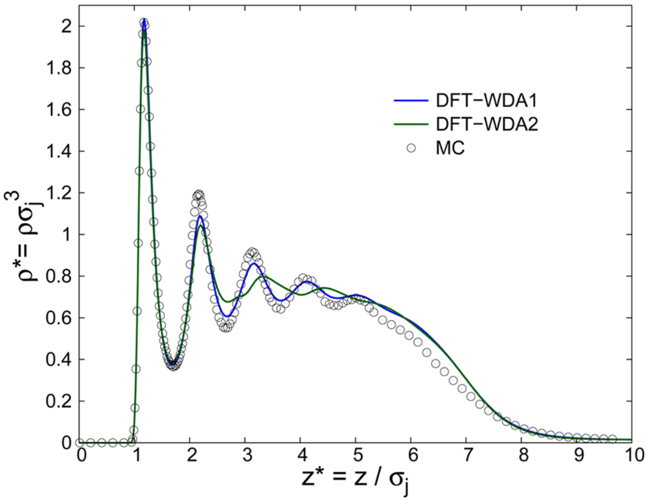

Figure 1. Density profile of a Lennard-Jones fluid forming a liquid film on a planar wall at $T^* = 0.9$ and $\mu_j^* = -4.45$ (corresponding PC-SAFT bulk phase pressure: $p^* = 0.011\,55$). Comparison between the DFT calculations of the variants WDA1 and WDA2 and results obtained by MC simulations.

Confined Systems. To demonstrate the transferability of the defined functional to confined systems, we show density profiles for a mixture of two Lennard-Jonesian components. The density profiles of grand-canonical MC simulations are taken from Sokolowski and Fischer.[90] The components are referred to as argon (a) and krypton (k) and defined by the parameters $\sigma_{aa} = 3.405$ Å, $\varepsilon_{aa}/k = 119.8$ K and $\sigma_{kk} = 3.630$ Å, $\varepsilon_{kk}/k = 163.1$ K, respectively. The external potential used by Sokolowski and Fischer[90] is identical to the potential in eq 10, with solid−fluid parameters $\sigma_{as} = 0.5621\sigma_a$, $\varepsilon_{as} = 23.998\varepsilon_a$, $\sigma_{bs} = 0.588\sigma_a$, and $\varepsilon_{bs} = 31.630\varepsilon_{aa}$. The slit-shaped geometry of the pore in this system is defined by a wall distance of $H = 5\sigma_{aa}$.

To obtain DFT density profiles of the binary mixture, two PC-SAFT components are defined by $m_a = 1$, σ_{aa}, ε_{aa} and $m_k = 1$, σ_{kk}, ε_{kk}, respectively. The DFT calculation was performed using the same external potential and wall distance.[90] The required chemical potentials $\mu_a^{\mathrm{res,b}}$ and $\mu_k^{\mathrm{res,b}}$ are obtained by PC-SAFT EoS using the given[90] dimensionless bulk (index b) phase temperature $T^b = \frac{\varepsilon_{aa}}{k}T^{b,*}$, density $\rho^b = \rho^{b,*}\sigma_{aa}^{-3}$ and mole fraction of argon x_a^b.

DFT density profiles and results from Sokolowski and Fischer[90] are shown for two different bulk phase conditions in Figure 2 and Figure 3. Only the left side of the profile is presented due to symmetry. In Figure 2, the adsorbed amount in the pore is significantly higher for krypton than for argon. The reason is that the krypton-solid attractive interaction is stronger and the (virtually) connected bulk phase consists of more krypton. In contrast, the system in Figure 3 is defined by a bulk phase with argon as dominant component which leads to a higher adsorption of argon relative to krypton.

The DFT density profiles are in very good agreement with the MC simulation data for both components and both bulk phase conditions. Density peaks and valleys are predicted

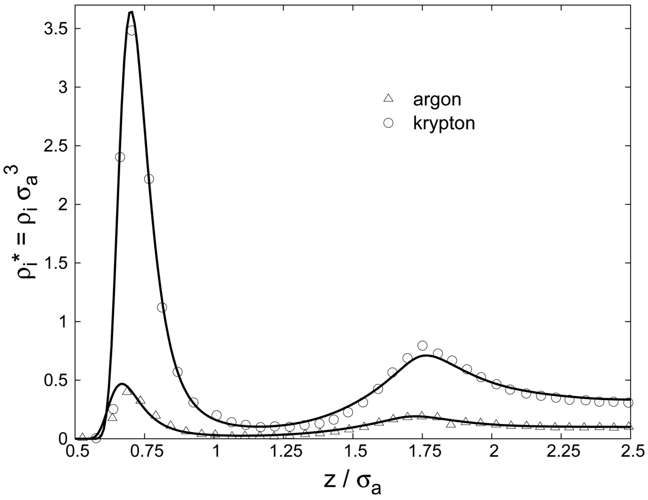

Figure 2. Density profile of a Lennard-Jones binary mixture in a slit-shaped pore at $T^* = 2.0$, $\rho^{b,*} = 0.444$, and $x_a^b = 0.262$. Comparison between the DFT calculations (full curve) and results obtained by MC simulations[90] (symbols).

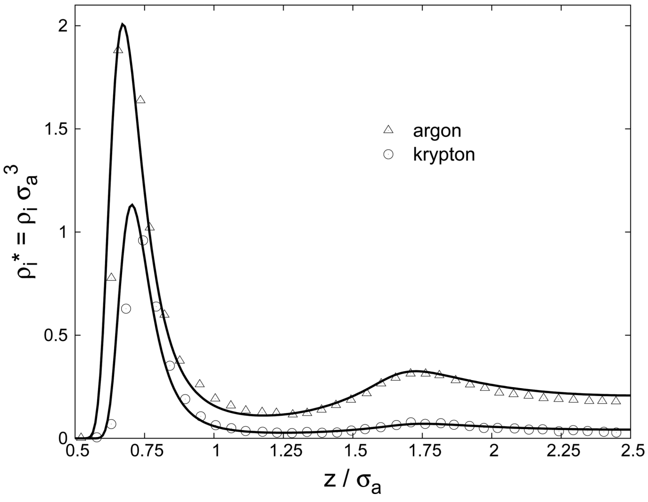

Figure 3. Density profile of a Lennard-Jones binary mixture in a slit-shaped pore at $T^* = 2.0$, $\rho^{b,*} = 0.103$, and $x_a^b = 0.891$. Comparison between the DFT calculations (full curve) and results obtained by MC simulations[90] (symbols).

accurately. These purely predictive results show that the model constant ψ obtained from experimental *n*-alkane surface tensions is transferable.

We now proceed to analyze nonmonoatomic (molecular) fluids. We consider ethane using the Transferable Anisotropic Mie (TAMie)[91] force field. The TAMie model represents fluid phase properties, in particular vapor−liquid equilibria, of ethane in good agreement with experimental data. Ethane is in this force field regarded as two Mie-interaction sites, representing the CH_3-groups a fixed bond-length apart. Such a model can also be referred to as "fused dimer" model. The molecular model of the PCP-SAFT EoS, on the other hand, is well-defined for integer values of segment number m_i. For noninteger values $1 < m_i < 2$, the equation of state is in excellent quantitative agreement to a fused dimer model.[75] A geometric interpretation for cases $1 < m_i < 2$, however, can not be given and we can therefore not expect DFT to represent accurately the density profile ($\rho(\mathrm{r})$) of the fused dimer model. We take molecular simulations for the TAMie model as a reference and compare results of the DFT approach to evaluate the quality of the dispersion functional.

We regard ethane in a slit-shaped pore. In the MC simulation, the pore is modeled by the external potential $V_{js}^{\mathrm{ext,MC}}$ using the 10,4,3 potential. The interaction parameters σ_{js} and ε_{js} in eq 11 are calculated with the Berthelot−Lorentz combining rules using the graphite solid phase parameters and the TAMie force field parameters of the ethane methyl bead: $\sigma_{jj} = 3.6463$ Å and $\varepsilon_{jj}/k = 130.78$ K. The MC simulations are performed in grand-canonical ensemble with a box size of 100 Å in *x*- and *y*-direction and a wall separation distance of $H = 36$ Å in *z*-direction. To omit cutoff corrections, the cutoff radius is defined to $r_c = 50$ Å. The number of particles in the simulation box varies during the simulation between 2980 and 3120. A number of 500 Δz slabs are used to sample the density profile.

In the MC simulations, the solid wall acts as an external potential on each interaction-site of ethane molecules. Within the DFT and PCP-SAFT EoS framework, the external potential describes the interaction between the solid wall and the entire molecule. The external potential used in the DFT calculations has to be multiplied by the number of segments, which leads to $V_{js}^{\mathrm{ext,DFT}} = 2V_{js}^{\mathrm{ext,MC}}$ in the case of ethane. The ethane pure component parameters for the DFT calculation are taken from Gross and Sadowski.[23]

The density profiles for both calculations are depicted in Figure 4 for the left side of the symmetric system. The figure shows segment density profiles, i.e., the probability of finding a CH_3-interaction site of ethane within a Δz slab. The MC simulation gives density profiles of these interaction sites due to the direct sampling of bead positions. In contrast, the DFT calculation initially provides molecular density profiles. To obtain the segment density profile of the DFT calculation, the molecular density profile is multiplied with the number of segments, i.e., factor 2.

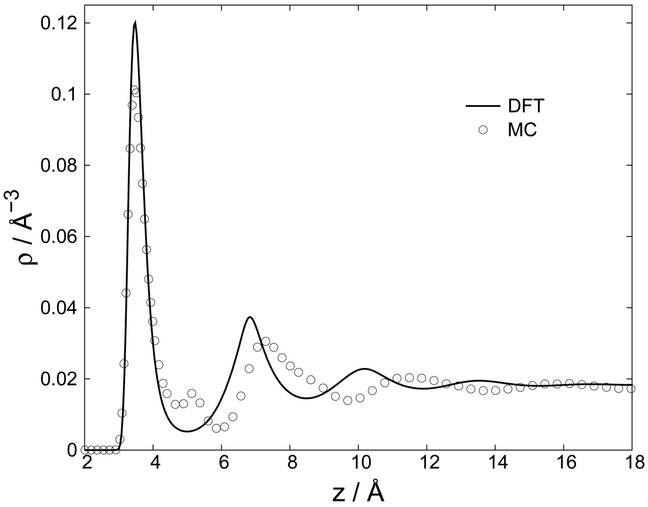

Figure 4. Density profile of methyl segments of ethane in a slit-shaped pore at $T = 250$ K and $\mu_j^* = \mu_j/kT - 3\ \ln(\Lambda_j/\text{Å}) = -8.15$ (corresponding PC-SAFT bulk phase pressure: 11.61 bar). Comparison between the DFT calculation and results obtained by the MC simulation using the TAMie[91] force field.

It is obvious that the profiles do not coincide. The main reason is the significant difference between the molecular models mentioned above. The "fused dimer" model of the

TAMie force field leads to the small peak at position 5.1 Å. At this location, methyl beads are sampled that are bound to a methyl bead located at position 3.5 Å, which is the tallest peak. The second small peak is due to ethane molecules oriented perpendicular to the solid wall. For the PCP-SAFT EoS, the segments of an ethane molecule oriented perpendicular to the solid wall give a contribution to the density profile at position of the first peak at 3.5 Å and the second peak at 7 Å, due to the tangentially bonding of segments. Therefore, finding a methyl bead at position 7 Å is more probable for the DFT calculation based on the PCP-SAFT EoS.

The different molecular models do not allow for same density profiles. Nonetheless, the presented functional gives a very good prediction of the adsorbed amount within the slit-shaped pore. The integration over the pore space leads to an averaged segment density

$$\rho_{\mathrm{av}} = \frac{1}{H}\int_0^H \rho(z)\mathrm{d}z \tag{36}$$

with values of $\rho_{\mathrm{av}}^{\mathrm{MC}} = 0.017\,02$ Å^{-3} and $\rho_{\mathrm{av}}^{\mathrm{DFT}} = 0.017\,78$ Å^{-3}, respectively. The result can in particular be appreciated when realizing that the corresponding (equilibrium) bulk phase at the same temperature and chemical potential is a vapor phase with a much lower bulk segment density of $\rho^{\mathrm{b}} = 0.000\,81$ Å^{-3}. The strong attractive interaction between fluid and solid phase leads to the formation of a liquid-like phase within the slit-shaped pore.

Repeating the DFT calculation for various chemical potentials μ_j^* leads to the adsorption isotherm depicted in Figure 5. In a certain range of μ_j^*, the calculated DFT density profile depends on the defined starting profile, leading to an apparent hysteresis phenomenon. We investigated the system similar to the procedure presented by Kierlik et al.[92] to obtain three different curves: By mimicking a pore filling process by increasing the chemical potential starting from a small value leads to results of the adsorption path. The reverse way gives the desorption path curve. The actual thermodynamic equilibrium for each μ_j^* corresponds to the minimal grand potential. The results show that the DFT prediction is in very good agreement with MC data over the entire region of chemical potential.

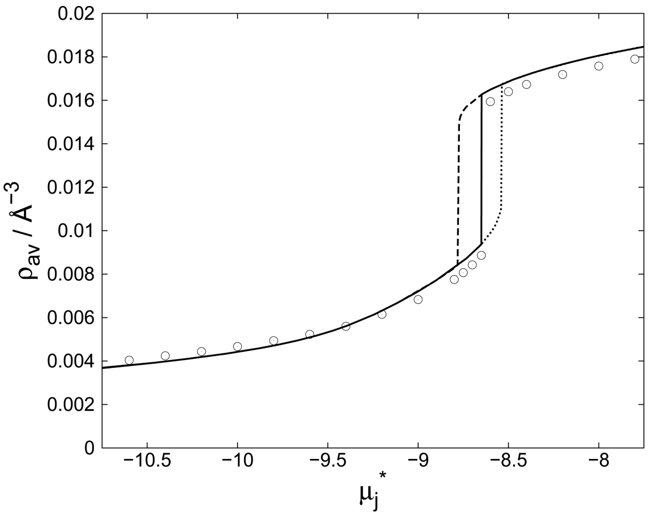

Figure 5. Adsorption isotherm of methyl segments of ethane in a slit-shaped pore at T = 250 K. Comparison between MC simulation (symbols) and DFT results: adsorption path (dotted curve), desorption path (dashed curve), and thermodynamic equilibrium (continuous curve).

Interfacial Tensions. In this section, we compare interfacial tensions as calculated from DFT with experimental values. In the previous section, we found the WDA1 variant of the dispersion contribution to the Helmholtz energy functional to be superior and thus use this variant for all calculations henceforth. The model parameter ψ was adjusted to n-alkanes and is subsequently treated as a universal model constant. Calculated surface tensions of most of the n-alkanes that were considered in identifying the ψ value are shown in Figure 6.

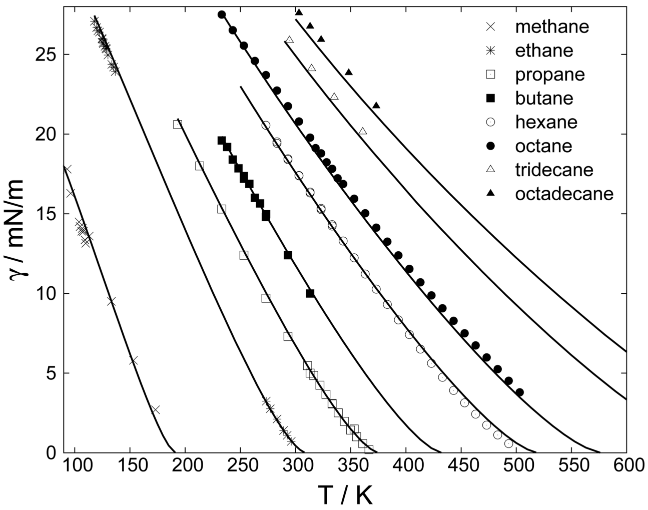

Figure 6. Surface tensions of several n-alkanes. Comparison between DFT calculations (full curve) and experimental data[86] (symbols).

The calculated surface tensions correlate the experimental data very accurately over a wide temperature range. We summarize the pure component parameters in the Supporting Information.

It is expected that the n-alkanes are well described by the proposed Helmholtz energy functional because a model parameter was adjusted to this class of substances. It is now interesting to assess how other substances are predicted. We consider one nonpolar and three polar components: 2,3-dimethylpentane, dimethyl ether, diethyl ether, and benzene in Figure 7. Dipole−dipole interactions are taken into account for the ether components and quadrupole−quadrupole interactions for benzene. The PCP-SAFT EoS overestimates the critical point somewhat. This leads to some deviations when approaching the critical temperature, as seen for dimethyl ether and benzene in Figure 7. Overall, however, all four components are predicted in very good agreement to experimental data over the range of temperature, in particular considering that no parameters were adjusted to interfacial properties for these substances.

Further, we compare interfacial tensions of binary mixtures that were presented in earlier work.[63,64] We first consider vapor−liquid systems and start with a mixture of small, almost spherical substances. The surface tension of a binary mixture of carbon monoxide (CO) and methane at vapor−liquid equilibrium conditions, at T = 90.67 K, is presented in Figure 8. The binary interaction parameter k_{ij} = 0.018 was adjusted to experimental VLE data.[63] Small deviations of calculated surface tensions from experimental data can be observed for both pure component boundaries and for the mixture. Nonetheless, we

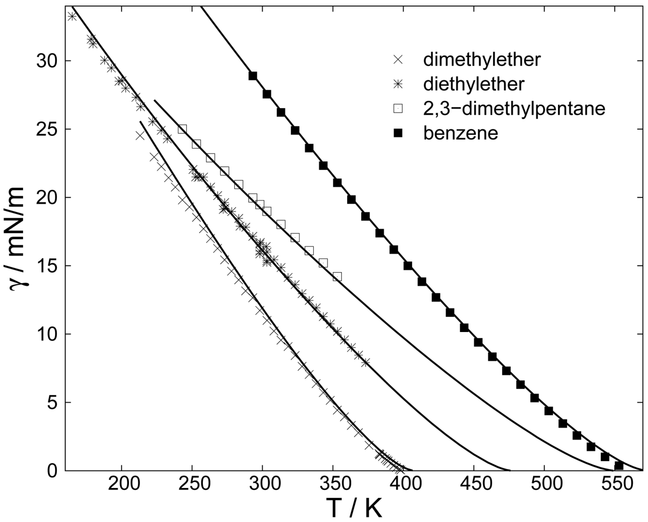

Figure 7. Surface tensions of various pure components. Comparison between DFT calculations (full curve) and experimental data (symbols) of dimethyl ether,[93,94] diethyl ether,[95−97] 2,3-dimethylpentane,[86] and benzene.[98]

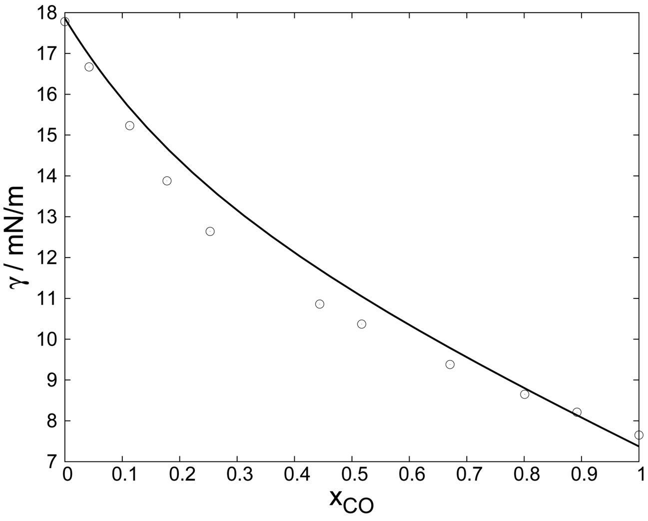

Figure 8. VLE surface tensions over the liquid-phase mole fraction x_{CO} of the CO−methane mixture at T = 90.67 K. Comparison between DFT calculations (full curve) and experimental data[99] (symbols).

assess the agreement of the DFT-predictions with experimental data as good because no parameter is adjusted to interfacial properties. Corresponding density profiles of the CO−CH_4 system are provided as Supporting Information.

Carbon monoxide is a mildly dipolar substance. Tetrahydrofuran (THF) is significantly more polar, and we consider the mixture of THF with *n*-hexane. Surface tensions of this binary mixture are shown Figure 9, where the binary interaction parameter k_{ij} = 0.012 was taken from ref 63. The surface tensions are in very good agreement over the entire range of THF composition. The results suggest the Helmholtz energy functional is suited for predicting the interfacial properties of polar mixtures.

The surface tension of *n*-hexane−*n*-dodecane, as a binary mixture of nonspherical, asymmetric species, is shown in Figure 10. The binary interaction parameter between *n*-hexane and *n*-dodecane was set to zero. This predictive calculation leads to a good description of the experimental values.

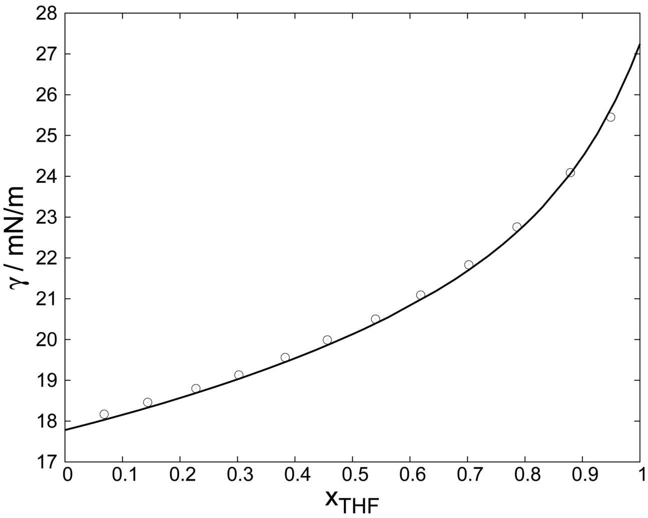

Figure 9. VLE surface tensions over the liquid-phase mole fraction x_{THF} of the THF-*n*-hexane mixture at T = 298.15 K. Comparison between DFT calculations (full curve) and experimental data[100] (symbols).

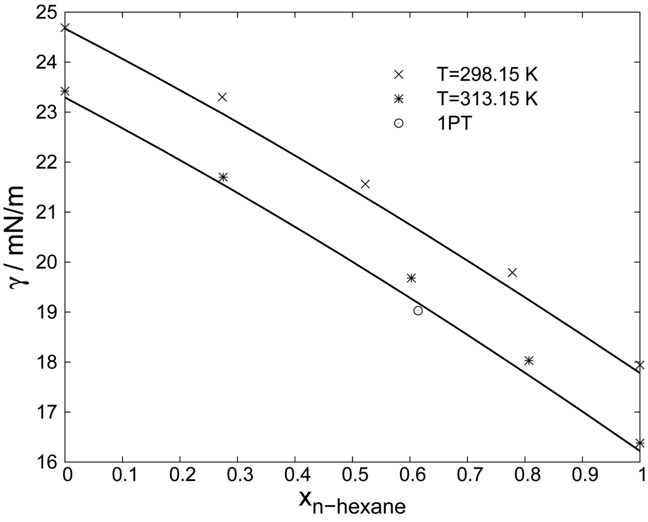

Figure 10. VLE surface tensions over the liquid-phase mole fraction $x_{n\text{-hexane}}$ of the *n*-hexane−*n*-dodecane mixture at T = 298.15 K and T = 313.15 K. Comparison between DFT calculations (full curve) and experimental data[101] (symbols).

Predicting the interfacial properties of liquid−liquid systems is particularly demanding. Analogous to Klink et al.,[64] we apply the presented WDA dispersion functional to interfacial tensions of LLE for binary mixtures of ethylene glycol with various solvents at T = 293.15 K and p = 1.013 bar. Ethylene glycol is modeled as a dipolar and associating substance. We use the same binary interaction parameters k_{ij} and l_{ij} as proposed by Klink et al.[64] to describe the LLE systems. According to Tang and Gross,[102] the l_{ij} parameter can be included via an expansion of the first order term of the dispersion contribution of the PCP-SAFT EoS. This expansion is used to calculate the LLE interfacial tensions shown in Figure 11. The agreement of the predicted interfacial tensions to experimental values is very satisfying considering that no parameter has been adjusted to interfacial properties. The results indicate that the suggested Helmholtz energy functional is able to predict rather complex

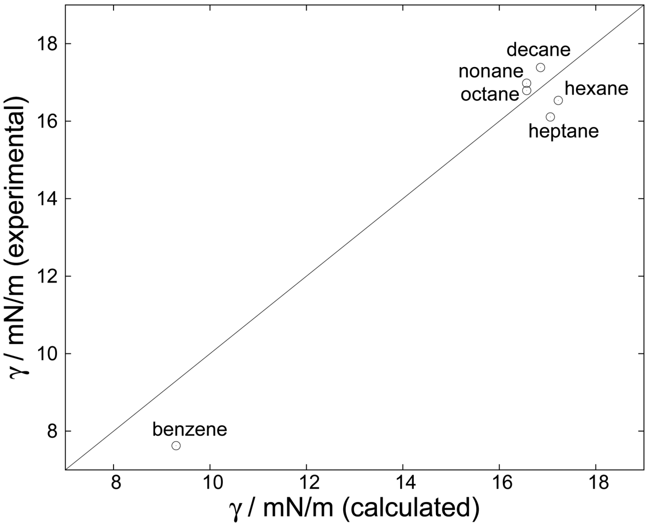

Figure 11. LLE interfacial tensions of ethylene glycol binary mixtures at T = 293.15 K and p = 1.013 bar. Comparison between DFT calculations and experimental data.[103]

binary mixtures, with significant associative and dipole−dipole interactions.

In Figure 10, we have shown a comparison between DFT results obtained with the here proposed Helmholtz energy functional and the functional proposed by members of our group earlier (1PT). The results are very similar. That similarity also holds for most other pure component and mixture interfacial tensions presented in this work. The corresponding surface tension to this density profiles are 19.19 and 19.03 mN/m for the DFT-1PT and the DFT-WDA1 approach, respectively. The suggested dispersion contribution F^{disp} performs comparable to the dispersion contribution F^{1PT} of the earlier works[62−64] in terms of interfacial tensions, however, with a much simpler Helmholtz energy functional. The simplicity of the Helmholtz energy functional is advantageous in three aspects: The functional is easier to implement and may facilitate the application of DFT approaches to various applications. Second, the calculation efficiency is much higher, with a typical calculation time of 4 s for the new functional, versus 300 s for the previous functional on a standard desktop computer. Lastly, the newly proposed functional is suitable for solid−fluid interfaces and the confined geometries that result from the solid structures.

CONCLUSION

Two variants of a dispersion contribution to the Helmholtz energy functional based on a WDA were presented. The resulting DFT model is applicable to confined systems and to fluid−liquid interfaces of mixtures. The two variants were compared and the superior variant was chosen. The local density of thin liquid adsorbed layer of a few molecular diameters thickness was particularly meaningful to discriminate between competing Helmholtz energy functionals. Calculated density profiles of fluids in slit-shaped pores show good agreement with density profiles obtained by MC simulations. Accurate results are found for the calculation of interfacial tensions. Pure components and mixtures with vapor−liquid and liquid−liquid interfaces were studied.

APPENDIX A: FUNCTIONAL DERIVATIVES

Equation 4 requires the functional derivative of the residual Helmholtz energy for a multicomponent system. In this appendix, the derivatives of all considered Helmholtz energy contributions according to eq 13 are presented for cylindrical coordinate systems where the density profiles vary only along the z-coordinate.

1. The Hard-Sphere Contribution

The derivative of the FMT functional[39,40] is given by

$$\begin{aligned}\frac{\delta F^{\text{hs}}[\rho_k]/\text{kT}}{\delta\rho_j(z^*)} &= m_j\int_{-d_j/2}^{d_j/2}\left(\frac{1}{d_j}\frac{\partial\Phi}{\partial n_0}+\frac{1}{2}\frac{\partial\Phi}{\partial n_1}+\pi d_j\frac{\partial\Phi}{\partial n_2}\right.\\ &\quad\left.+\pi\frac{\partial\Phi}{\partial n_3}\left[\left(\frac{d_j}{2}\right)^2-\hat{z}^2\right]\right)\text{d}\hat{z}\\ &\quad+\mathbf{e}_z m_j\int_{-d_j/2}^{d_j/2}\left(\frac{1}{d_j}\frac{\partial\Phi}{\partial\mathbf{n}_1}+2\pi\frac{\partial\Phi}{\partial\mathbf{n}_2}\right)\hat{z}\text{d}\hat{z}\end{aligned} \tag{37}$$

where d_j the temperature dependent segment diameter and $\mathbf{e}_z$ the unit vector that points in z-direction. n_α are the scalar and $\mathbf{n}_\alpha$ are the vector weighted densities and calculate as

$$n_0(z) = \sum_i^{N_c} m_i\frac{1}{d_i}\int_{-d_i/2}^{d_i/2}\rho_i(z+\hat{z})\text{d}\hat{z} \tag{38}$$

$$n_1(z) = \frac{1}{2}\sum_i^{N_c} m_i\int_{-d_i/2}^{d_i/2}\rho_i(z+\hat{z})\text{d}\hat{z} \tag{39}$$

$$n_2(z) = \pi\sum_i^{N_c} m_i d_i\int_{-d_i/2}^{d_i/2}\rho_i(z+\hat{z})\text{d}\hat{z} \tag{40}$$

$$n_3(z) = \pi\sum_i^{N_c} m_i\int_{-d_i/2}^{d_i/2}\rho_i(z+\hat{z})\left[\left(\frac{d_i}{2}\right)^2-\hat{z}^2\right]\text{d}\hat{z} \tag{41}$$

$$\mathbf{n}_1(z) = -\mathbf{e}_z\sum_i^{N_c} m_i\frac{1}{d_i}\int_{-d_i/2}^{d_i/2}\rho_i(z+\hat{z})\hat{z}\text{d}\hat{z} \tag{42}$$

$$\mathbf{n}_2(z) = -2\pi\mathbf{e}_z\sum_i^{N_c} m_i\int_{-d_i/2}^{d_i/2}\rho_i(z+\hat{z})\hat{z}\text{d}\hat{z} \tag{43}$$

Note that the negative sign in eqs 42 and 43 is required and that we erroneously omitted the sign in the corresponding equation in our previous work.[62] The partial derivation of the Helmholtz energy functional Φ with respect to all n_α and $\mathbf{n}_\alpha$ provides

$$\frac{\partial\Phi}{\partial n_0} = -\ln(1-n_3) \tag{44}$$

$$\frac{\partial\Phi}{\partial n_1} = \frac{n_2}{1-n_3} \tag{45}$$

$$\begin{aligned}\frac{\partial\Phi}{\partial n_2} &= \frac{n_1}{1-n_3}+3(n_2^2-\mathbf{n}_2\cdot\mathbf{n}_2)\\ &\quad\times\frac{n_3+(1-n_3)^2\ln(1-n_3)}{36\pi n_3^2(1-n_3)^2}\end{aligned} \tag{46}$$

$$\frac{\partial \Phi}{\partial n_3} = \frac{n_0}{1-n_3} + \frac{n_1 n_2 - \mathbf{n}_1 \cdot \mathbf{n}_2}{(1-n_3)^2} - (n_2^3 - 3 n_2 \mathbf{n}_2 \cdot \mathbf{n}_2) \times \frac{n_3(n_3^2 - 5n_3 + 2) + 2(1-n_3)^3 \ln(1-n_3)}{36\pi n_3^3 (1-n_3)^3} \tag{47}$$

$$\frac{\partial \Phi}{\partial \mathbf{n}_1} = -\frac{\mathbf{n}_2}{1-n_3} \tag{48}$$

$$\frac{\partial \Phi}{\partial \mathbf{n}_2} = -\frac{\mathbf{n}_1}{1-n_3} - n_2 \mathbf{n}_2 \frac{n_3 + (1-n_3)^2 \ln(1-n_3)}{6\pi n_3^2 (1-n_3)^2} \tag{49}$$

2. The Chain Contribution

The functional derivative of the chain contribution is

$$\frac{\delta F^{\mathrm{hc}}[\rho_k]/\mathrm{kT}}{\delta \rho_j(z^*)} = -(m_j - 1)\left(\ln \frac{y_{jj}^{\mathrm{dd}}(\overline{\rho}_k^{\mathrm{hc}}(z^*))\lambda_j(z^*)}{\rho_j(z^*)} - 1\right) \tag{50}$$

$$- \frac{3}{4d_j^3} \sum_i (m_i - 1) \int_{-d_j}^{d_j} \rho_i(z^* + \hat{z}) \tag{51}$$
$$\times \frac{\partial \ln y_{ii}^{\mathrm{dd}}}{\partial \overline{\rho}_j^{\mathrm{hc}}(z^* + \hat{z})}[d_j^2 - \hat{z}^2]\mathrm{d}\hat{z}$$

$$- \frac{1}{2d_j}(m_j - 1) \int_{-d_j}^{d_j} \frac{\rho_j(z^* + \hat{z})}{\lambda_j(z^* + \hat{z})}\mathrm{d}\hat{z} \tag{52}$$

where λ_i and $\overline{\rho}_i^{\mathrm{hc}}$ are weighted densities of the chain contribution

$$\lambda_i(z) = \frac{1}{2d_i} \int_{-d_i}^{d_i} \rho_i(z + \hat{z})\mathrm{d}\hat{z} \tag{53}$$

$$\overline{\rho}_i^{\mathrm{hc}}(z) = \frac{3}{4d_i^3} \int_{-d_i}^{d_i} \rho_i(z + \hat{z})[d_i^2 - \hat{z}^2]\mathrm{d}\hat{z} \tag{54}$$

3. The Contribution of Dispersive Attraction

The functional derivative of variant 1 reads

$$\frac{\delta F^{\mathrm{disp},1}[\rho_k]/\mathrm{kT}}{\delta \rho_j(z^*)} = \frac{3}{4\psi_1^3 d_j^3} \int_{-\psi_1 d_j}^{\psi_1 d_j} \left.\frac{\partial \overline{\rho}\, \tilde{a}^{\mathrm{disp}}}{\partial \overline{\rho}_j}\right|_{z^*+\hat{z}} [\psi_1^2 d_j^2 - \hat{z}^2]\mathrm{d}\hat{z} \tag{55}$$

and variant 2

$$\frac{\delta F^{\mathrm{disp},2}[\rho_k]/\mathrm{kT}}{\delta \rho_j(z^*)} = \tilde{a}^{\mathrm{disp}}(\overline{\rho}_k(z^*)) + \frac{3}{4\psi_2^3 d_j^3} \int_{-\psi_2 d_j}^{\psi_2 d_j} \rho(z^* + \hat{z}) \times \left.\frac{\partial \tilde{a}^{\mathrm{disp}}}{\partial \overline{\rho}_j}\right|_{z^*+\hat{z}} [\psi_2^2 d_j^2 - \hat{z}^2]\mathrm{d}\hat{z} \tag{56}$$

Note that the weighted density depends on the value of the universal parameter ψ

$$\overline{\rho}_i(z) = \frac{3}{4\psi^3 d_i^3} \int_{-\psi d_i}^{\psi d_i} \rho_i(z + \hat{z})[\psi^2 d_i^2 - \hat{z}^2]\mathrm{d}\hat{z} \tag{57}$$

4. The Multipolar Attraction

The functional derivative of the multipolar term uses the weighted density of eq 57

$$\frac{\delta F^{\mathrm{mp}}[\rho_k]/\mathrm{kT}}{\delta \rho_j(z^*)} = \tilde{a}^{\mathrm{mp}}(\overline{\rho}_k(z^*)) + \frac{3}{4\psi^3 d_j^3} \int_{-\psi d_j}^{\psi d_j} \rho(z^* + \hat{z}) \times \left.\frac{\partial \tilde{a}^{\mathrm{mp}}}{\partial \overline{\rho}_j}\right|_{z^*+\hat{z}} [\psi^2 d_j^2 - \hat{z}^2]\mathrm{d}\hat{z} \tag{58}$$

APPENDIX B: COMPARISON WITH SHEN ET AL

The structure of the dispersion functional presented by Shen et al.[67] is similar to the WDA2 variant. Fore pure components, the functional of Shen et al. coincides with WDA2 for $\psi_{\mathrm{WDA2}} = 1.5$. Figure 12 compares the WDA1 and the Shen et al. functional applied to the adsorbed liquid-like film presented in Figure 1 of the main text. The WDA1 functional proposed above is in better agreement to the results from molecular simulation data. We note, however, that both functionals showed rather small differences for many other systems.

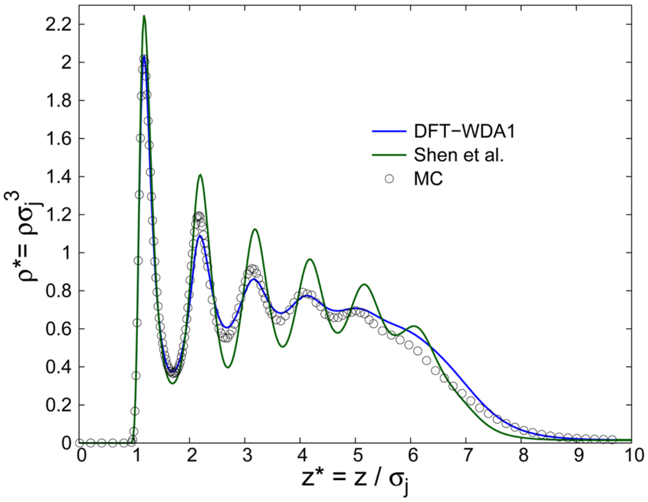

Figure 12. Density profile of a Lennard-Jones fluid forming a liquid film on a planar wall at $T^* = 0.9$ and $\mu_j^* = -4.45$.

APPENDIX C: DERIVATION OF THE WEIGHTED DENSITY FORMALISM

We show a derivation of the weighted density formalism for the Helmholtz energy functional, similar to the work of Curtin and Ashcroft.[83] We recapitulate this derivation to show the formalism for multi component systems and to emphasize important assumptions required along the development. We start with an exact Helmholtz energy functional for an inhomogeneous system and assess what assumptions are required to bring a WDA functional into agreement with the exact functional.

We divide the intermolecular pair potential ϕ_{ij} between molecule i and j into a reference part ϕ_{ij}^{ref} and a perturbation contribution ϕ_{ij}^{PT}, as

$$\phi_{\lambda,ij}(|\mathbf{r}_1 - \mathbf{r}_2|) = \phi_{ij}^{\mathrm{ref}}(|\mathbf{r}_1 - \mathbf{r}_2|) + \lambda \phi_{ij}^{\mathrm{PT}}(|\mathbf{r}_1 - \mathbf{r}_2|) \tag{59}$$

where the coupling parameter λ is introduced to allow a smooth transition between the reference fluid ($\lambda = 0$) and the target fluid, with $\phi_{ij} = \phi_{\lambda=1,ij}$ for $\lambda = 1$. Here, we regard $\mathbf{r}_1$ as generalized coordinates for molecules of type i, detailing the position, orientation, and conformation. For simplicity and without considerable loss of detail, however, we can consider simple spherically symmetric substances such as argon or spherical segments of a chain molecule. An exact expression for the perturbation part of the Helmholtz energy[71] (of a multicomponent inhomogeneous system) is

$$\frac{F^{\mathrm{PT}}[\rho_k]}{kT} = \frac{1}{2}\sum_i \sum_j \int\int \frac{\phi_{ij}^{\mathrm{PT}}(|\mathbf{r}_1 - \mathbf{r}_2|)}{kT} \int_0^1 \rho_{\lambda,\mathrm{ij}}^{(2)}(\mathbf{r}_1, \mathbf{r}_2)\mathrm{d}\lambda \mathrm{d}\mathbf{r}_2 \mathrm{d}\mathbf{r}_1 \tag{60}$$

where $\rho_{\lambda,ij}^{(2)}(\mathbf{r}_1, \mathbf{r}_2)$ is the two-body density of two molecules defined by the intermediate potential $\phi_{\lambda,ij}(|\mathbf{r}_1 - \mathbf{r}_2|)$. The intermolecular two-body density $\rho_{\lambda,\mathrm{ij}}^{(2)}(\mathbf{r}_1, \mathbf{r}_2)$ is related to the pair correlation function $g_{\lambda,ij}(\mathbf{r}_1, \mathbf{r}_2)$ by

$$\rho_{\lambda,\mathrm{ij}}^{(2)}(\mathbf{r}_1, \mathbf{r}_2) = \rho_i(\mathbf{r}_1)\rho_j(\mathbf{r}_2) g_{\lambda,\mathrm{ij}}(\mathbf{r}_1, \mathbf{r}_2) \tag{61}$$

Inserting eq 61 into eq 60 and changing the sequence of summation and integration leads to

$$\frac{F^{\mathrm{PT}}[\rho_k]}{kT} = \frac{1}{2}\sum_i \int \rho_i(\mathbf{r}_1) \sum_j \int \rho_j(\mathbf{r}_2) \frac{\phi_{ij}^{\mathrm{PT}}(|\mathbf{r}_1 - \mathbf{r}_2|)}{kT} \int_0^1 g_{\lambda,\mathrm{ij}}(\mathbf{r}_1, \mathbf{r}_2)\mathrm{d}\lambda \mathrm{d}\mathbf{r}_2 \mathrm{d}\mathbf{r}_1 \tag{62}$$

We realize, that F^{PT} can be formulated compactly as

$$\frac{F^{\mathrm{PT}}[\rho_k]}{kT} = \sum_i \int \rho_i(\mathbf{r}_1) \tilde{a}_i^{\mathrm{PT}}[\rho_k; \mathbf{r}_1] \mathrm{d}\mathbf{r}_1 \tag{63}$$

by defining a reduced Helmholtz energy $\tilde{a}_i^{\mathrm{PT}}$, which is itself a functional and is related to component i and position $\mathbf{r}_1$

$$\tilde{a}_i^{\mathrm{PT}}[\rho_k; \mathbf{r}_1] = \frac{1}{2}\sum_j \int \rho_j(\mathbf{r}_2) \frac{\phi_{ij}^{\mathrm{PT}}(|\mathbf{r}_1 - \mathbf{r}_2|)}{kT} \int_0^1 g_{\lambda,\mathrm{ij}}(\mathbf{r}_1, \mathbf{r}_2)\mathrm{d}\lambda \mathrm{d}\mathbf{r}_2 \tag{64}$$

For bulk systems, $\tilde{a}_i^{\mathrm{PT}}$ simplifies to a function

$$\begin{aligned} \tilde{a}_i^{\mathrm{PT,b}}(\rho_k^{\mathrm{b}}) &= \frac{1}{2}\sum_j \rho_j^{\mathrm{b}} \int \frac{\phi_{ij}^{\mathrm{PT}}(|\mathbf{r}_1 - \mathbf{r}_3|)}{kT} \int_0^1 g_{\lambda,\mathrm{ij}}^{\mathrm{b}}(|\mathbf{r}_1 - \mathbf{r}_3|, \rho_k^{\mathrm{b}})\mathrm{d}\lambda \mathrm{d}\mathbf{r}_3 \\ &= \frac{1}{2}\sum_j \rho_j^{\mathrm{b}} K_{ij}^{\mathrm{b}}(\rho_k^{\mathrm{b}}, T) \end{aligned} \tag{65}$$

with the radial distribution function $g_{\lambda,ij}^{\mathrm{b}}(r)$ as a function of the particle distance r, bulk partial densities ρ_k^{b}, and temperature T. Of course, even for simple intermolecular potential functions, the radial distribution function $g_{\lambda,ij}^{\mathrm{b}}(r)$ is not available for arbitrary values of λ. Note that position $\mathbf{r}_1$ has no influence in eq 65 due to the homogeneity of bulk phases. To keep the further derivation neat, we have introduced the abbreviation K_{ij}^{b} and renamed the integration variable $\mathbf{r}_2$ into $\mathbf{r}_3$.

In what follows, we set the reduced Helmholtz energy $\tilde{a}_i^{\mathrm{PT,b}}$ to be equal to the full expression $\tilde{a}_i^{\mathrm{PT}}[\rho_k; \mathbf{r}_1]$ and deduce appropriate definitions of averaged densities, referred to as weighted densities, which capture the inhomogeneous density profile around a given position $\mathbf{r}_1$ appropriately. For the weighted densities, we adopt the general formulation in eq 15. Inserting the weighted densities into the bulk formulation of the reduced Helmholtz energy, eq 65, leads to

$$\tilde{a}_i^{\mathrm{PT,b}}(\bar{\rho}_k(\mathbf{r}_1)) = \frac{1}{2}\sum_j \bar{\rho}_j(\mathbf{r}_1) K_{ij}^{\mathrm{b}}(\bar{\rho}_k(\mathbf{r}_1), T) \tag{66}$$

where K_{ij}^{b} as well as $\bar{\rho}_j$ are related to position $\mathbf{r}_1$. We insert eq 15, and obtain

$$\begin{aligned} \tilde{a}_i^{\mathrm{PT,b}}(\bar{\rho}_k(\mathbf{r}_1)) &= \frac{1}{2}\sum_j \int \rho_j(\mathbf{r}_2) w_j(|\mathbf{r}_1 - \mathbf{r}_2|)\mathrm{d}\mathbf{r}_2 \cdot K_{ij}^{\mathrm{b}}(\bar{\rho}_k(\mathbf{r}_1), T) \\ &= \frac{1}{2}\sum_j \int \rho_j(\mathbf{r}_2) w_j(|\mathbf{r}_1 - \mathbf{r}_2|) K_{ij}^{\mathrm{b}}(\bar{\rho}_k(\mathbf{r}_1), T)\mathrm{d}\mathbf{r}_2 \end{aligned} \tag{67}$$

The correlation integral K_{ij}^{b} is independent of $\mathbf{r}_2$ and we moved it into the $\mathbf{r}_2$ integral. An appropriate definition of w_i is found, when the weighted density version of the reduced Helmholtz energy, eq 67, is brought to agreement with the exact form of the reduced Helmholtz energy of the inhomogeneous system, eq 64, requiring $\tilde{a}_i^{\mathrm{PT}}[\rho_k; \mathbf{r}_1] = \tilde{a}_i^{\mathrm{PT,b}}(\bar{\rho}_k(\mathbf{r}_1))$ for all considered components i and for the entire integration space of $\mathbf{r}_1$. We get

$$\begin{aligned} &\frac{1}{2}\sum_j \int \rho_j(\mathbf{r}_2) \frac{\phi_{ij}^{\mathrm{PT}}(|\mathbf{r}_1 - \mathbf{r}_2|)}{kT} \int_0^1 g_{\lambda,\mathrm{ij}}(\mathbf{r}_1, \mathbf{r}_2)\mathrm{d}\lambda \mathrm{d}\mathbf{r}_2 \\ &= \frac{1}{2}\sum_j \int \rho_j(\mathbf{r}_2) w_j(|\mathbf{r}_1 - \mathbf{r}_2|) K_{ij}^{\mathrm{b}}(\bar{\rho}_k(\mathbf{r}_1), T)\mathrm{d}\mathbf{r}_2 \end{aligned} \tag{68}$$

and obtain the definition of w_j as

$$\begin{aligned} &w_j(|\mathbf{r}_1 - \mathbf{r}_2|) \\ &= \frac{\phi_{ij}^{\mathrm{PT}}(|\mathbf{r}_1 - \mathbf{r}_2|) \int_0^1 g_{\lambda,\mathrm{ij}}(\mathbf{r}_1, \mathbf{r}_2)\mathrm{d}\lambda}{\int \phi_{ij}^{\mathrm{PT}}(|\mathbf{r}_1 - \mathbf{r}_3|) \int_0^1 g_{\lambda,\mathrm{ij}}^{\mathrm{b}}(|\mathbf{r}_1 - \mathbf{r}_3|, \bar{\rho}_k(\mathbf{r}_1))\mathrm{d}\lambda \mathrm{d}\mathbf{r}_3} \end{aligned} \tag{69}$$

We can see that the definition of a weight function is not unique for mixtures because this equation needs to hold for every component-index i. Only if eq 69 was satisfied for every (i, j)-pair and for all $\mathbf{r}_1$, $\mathbf{r}_2$ combinations, would eq 68 be exact. The assumption, that eq 69 is fulfilled is known (although in a slightly different way of writing) as the one-fluid theory.[104] The equation nonetheless rationalizes the development of reasonable WDA models for the dispersion contribution of the Helmholtz energy functional. To have a uniquely defined starting point for developing an approximate model, we only regard (j, j) correlations and interactions, as

$$\begin{aligned} &w_j(|\mathbf{r}_1 - \mathbf{r}_2|) \\ &= \frac{\phi_{jj}^{\mathrm{PT}}(|\mathbf{r}_1 - \mathbf{r}_2|) \int_0^1 g_{\lambda,\mathrm{jj}}(\mathbf{r}_1, \mathbf{r}_2)\mathrm{d}\lambda}{\int \phi_{jj}^{\mathrm{PT}}(|\mathbf{r}_1 - \mathbf{r}_3|) \int_0^1 g_{\lambda,\mathrm{jj}}^{\mathrm{b}}(|\mathbf{r}_1 - \mathbf{r}_3|, \bar{\rho}_k(\mathbf{r}_1))\mathrm{d}\lambda \mathrm{d}\mathbf{r}_3} \end{aligned} \tag{70}$$

We further assume that the results of both integrals in eq 70 are identical.

$$\int_0^1 g_{\lambda,\mathrm{jj}}^{\mathrm{b}}(|\mathbf{r}_1 - \mathbf{r}_3|, \bar{\rho}_k(\mathbf{r}_1))\mathrm{d}\lambda \approx \int_0^1 g_{\lambda,\mathrm{jj}}(\mathbf{r}_1, \mathbf{r}_2)\mathrm{d}\lambda \tag{71}$$

We can make an attempt to justify this assumption. If the weight function is defined appropriately, then the Helmholtz energy as a functional of the single particle density is accurately described. The two-particle density (and thus the radial distribution function) is the functional derivative of the Helmholtz energy with respect to the pair potential. Therefore, also the two-particle density is a functional of the same (appropriately defined) weighted density. If we construct a limiting case where a weight function leads to exact results, then also the two-particle density is accurately described (self-

DOI: 10.1021/acs.iecr.6b04551
Ind. Eng. Chem. Res. 2017, 56, 4119−4135

consistently) with the same appropriately defined weight function. As a consequence we conjecture: the better the weight function performs for the Helmholtz energy functional, the better the assumption, eq 71, gets. Our arguments so far do not justify that a bulk phase expression for radial distribution function can be used. This aspect is discussed in more detail in the work of Schulte et al.[105]

With the two approximations given above, the weight function simplifies to

$$w_j(|\mathbf{r}_1 - \mathbf{r}_2|) = \frac{\phi_{jj}^{\mathrm{PT}}(|\mathbf{r}_1 - \mathbf{r}_2|)}{\int \phi_{jj}^{\mathrm{PT}}(|\mathbf{r}_1 - \mathbf{r}_3|)\mathrm{d}\mathbf{r}_3} \tag{72}$$

Modeling of the Helmholtz Energy Using PC-SAFT EoS

In conclusion, we obtain the perturbation part of the Helmholtz energy of an inhomogeneous system as

$$\frac{F^{\mathrm{disp}}[\rho_k]}{kT} = \sum_i \int \rho_i(\mathbf{r}_1)\tilde{a}_i^{\mathrm{disp}}(\bar{\rho}_k(\mathbf{r}_1))\mathrm{d}\mathbf{r}_1 \tag{73}$$

with $\tilde{a}_i^{\mathrm{disp}}(\bar{\rho}_k(\mathbf{r}_1))$ as the reduced Helmholtz energy of the corresponding bulk phase calculated with the weighted densities at position $\mathbf{r}_1$. The weighted densities $\bar{\rho}_j(\mathbf{r}_1)$ are determined from eq 15 using the weight w_j defined in eq 72. At this point, we renamed $\tilde{a}_i^{\mathrm{PT,b}}$ into $\tilde{a}_i^{\mathrm{disp}}$ to illustrate, that we connect the dispersion functional to the PCP-SAFT EoS instead of performing eq 66. To determine $\tilde{a}_i^{\mathrm{disp}}$, we equate eq 73 for bulk phases with the PCP-SAFT Helmholtz energy of the dispersion contribution $F^{\mathrm{disp}}/kT = N\,\tilde{a}^{\mathrm{disp}}$, where $\tilde{a}^{\mathrm{disp}}$ is the dispersion contribution of PCP-SAFT. This leads to the desired relation between $\tilde{a}_i^{\mathrm{disp}}$ and $\tilde{a}^{\mathrm{disp}}$

$$\tilde{a}^{\mathrm{disp}}(\rho_k^{\mathrm{b}}) = \frac{V}{N}\sum_i \rho_i^{\mathrm{b}}\tilde{a}_i^{\mathrm{disp}}(\rho_k^{\mathrm{b}}) = \sum_i x_i^{\mathrm{b}}\tilde{a}_i^{\mathrm{disp}}(\rho_k^{\mathrm{b}}) \tag{74}$$

with the bulk phase mole fraction x_i^{b}. For $\tilde{a}^{\mathrm{disp}}$, we introduce the equation described by Gross and Sadowski,[23] and obtain for the component-wise additive reduced Helmholtz energy

$$\tilde{a}_i^{\mathrm{disp}}(\rho_k^{\mathrm{b}}) = -\pi m_i \sum_j \rho_j^{\mathrm{b}} m_j \sigma_{ij}^3 \frac{\varepsilon_{ij}}{kT}\left[2I_1 + \frac{\varepsilon_{ij}}{kT}\bar{m}C_1 I_2\right] \tag{75}$$

According to the WDA, $\tilde{a}_i^{\mathrm{disp}}$ must be evaluated as a function of locally defined weighted densities $\bar{\rho}_k(\mathbf{r}_1)$ to provide a description of inhomogeneous systems

$$\tilde{a}_i^{\mathrm{disp}}(\bar{\rho}_k(\mathbf{r}_1)) = -\pi m_i \sum_j \bar{\rho}_j(\mathbf{r}_1) m_j \sigma_{ij}^3 \frac{\varepsilon_{ij}}{kT}\left[2I_1(\bar{\eta}, \bar{m}) + \frac{\varepsilon_{ij}}{kT}\bar{m}C_1 I_2(\bar{\eta}, \bar{m})\right] \tag{76}$$

The calculation of $\bar{m}$, C_1, and $\bar{\eta}$ proceeds as shown in eqs 22, 24, and 25.

Definition of Weight Functions

To obtain a dispersion functional based on the PCP-SAFT EoS and the WDA, a definition of an appropriate weight w_j or, with eq 72, of a perturbation part of the intermolecular potential ϕ_{jj}^{PT} is required. The PCP-SAFT dispersion contribution $\tilde{a}^{\mathrm{disp}}$ is derived using the perturbation theory presented by Barker and Henderson[106,107] with a hard-chain fluid as reference system. A Lennard-Jones perturbing potential has been used with model constants adjusted to pure component properties of *n*-alkanes[23] (with the soft repulsion only roughly approximated through a step potential[108]). Therefore, a Lennard-Jones perturbing potential $\phi_{jj}^{\mathrm{PT,LJ}}$ is the most obvious choice for eq 72, leading to a Lennard-Jonesian weighted density $\bar{\rho}_j^{\mathrm{LJ}}$. Because substantial approximations have gone into eq 72, other choices are possible. A more short-ranged weight function is desirable for favorable computational efficiency. We tested the square-well (SW) potential, $\phi_{jj}^{\mathrm{PT,SW}}(r) = -\varepsilon_{jj}\,\Theta[\psi_{\mathrm{SW}}\,d_{jj} - r]\Theta[r - d_{jj}]$, with d_{jj} as the temperature-dependent effective repulsive (hard-sphere) diameter, and with ψ_{SW} as the well-width of the SW-potential. We have rewritten $\phi_{jj}^{\mathrm{PT,SW}}$ into a product of Heaviside functions Θ, leading (with eqs 72 and 15) to the SW weighted density, as

$$\bar{\rho}_j^{\mathrm{SW}}(\mathbf{r}_1) = \frac{3}{4\pi d_{jj}^3(\psi_{\mathrm{SW}}^3 - 1)}\int \rho_j(\mathbf{r}_2)\Theta[\psi_{\mathrm{SW}}d_{jj} - |\mathbf{r}_1 - \mathbf{r}_2|] \times \Theta[|\mathbf{r}_1 - \mathbf{r}_2| - d_{jj}]\mathrm{d}\mathbf{r}_2 \tag{77}$$

eq 77 states that $\bar{\rho}_j^{\mathrm{SW}}(\mathbf{r}_1)$ is evaluated by an averaging of uniformly weighted local densities within a spherical shell, where the shell is defined by the radii d_{jj} and $\psi_{\mathrm{SW}}\cdot d_{jj}$ and its center is at position $\mathbf{r}_1$.

An even simpler definition of the weighted density, namely a density-averaging in a sphere of diameter ψ around a considered position is obtained with the Heaviside weight, eq 16, was used in the main text of this work.

Remarks

The development in this appendix led to two additional dispersion functionals, beyond the two variants that were compared in the main text, i.e., the Helmholtz energy according to eq 73 evaluated with the weighted densities $\bar{\rho}_k^{\mathrm{SW}}$ and $\bar{\rho}_k^{\mathrm{LJ}}$, respectively. We adjusted the universal parameter ψ_{SW} of the SW approach to the surface tension of pure *n*-alkane, just as described above for the WDA1 and WDA2 approaches. The LJ approach has no adjustable parameter. Applying all functionals to confined systems, however, showed that the variants WDA1 and WDA2 are clearly superior to the SW and the LJ approaches, so that no further examination of the LJ and SW approach was made.

■ APPENDIX D: CHAIN CONTRIBUTION

To discuss the origin of eq 14, we look at the different definitions of the ideal gas reference state of the PCP-SAFT and the Tripathi and Chapman[45,46] formalism, respectively. The PCP-SAFT EoS defines the ideal gas state for a mixture of chain molecules, eq 5, as reference state. F^{id} of real molecules can either be estimated from quantum mechanical calculations[109] or it can be obtained from experimental data on ideal gas heat capacities. The native reference state according to Wertheim's theory, like in the work of Tripathi and Chapman, is defined by an ideal gas of nonbonded segments, with the Helmholtz energy functional

$$\frac{F^{\mathrm{ID}}[\rho_k]}{kT} = \sum_i \sum_{\alpha_i}^{m_i} \int \rho_{\alpha_i}(\mathbf{r})\{\ln(\rho_{\alpha_i}(\mathbf{r})\Lambda_{\alpha_i}^3) - 1\}\mathrm{d}\mathbf{r} \tag{78}$$

where the sum α_i runs over all segments in molecule *i*. Capital-letter superscripts denote the Tripathi and Chapman formalism. The molecular density is defined as a local average of all segment densities

$$\rho_i(\mathbf{r}) = \frac{1}{m_i}\sum_{\alpha_i}^{m_i} \rho_{\alpha_i}(\mathbf{r}) \tag{79}$$

For the case, where the segment density profiles are averaged, it follows that $\rho_i(\mathbf{r}) = \rho_{\alpha i}(\mathbf{r})$ and one gets

$$\frac{F^{\mathrm{ID}}[\rho_k]}{kT} = \sum_i m_i \int \rho_i(\mathbf{r})\{\ln(\rho_i(\mathbf{r})\Lambda_{s,i}^3) - 1\}\mathrm{d}\mathbf{r} \tag{80}$$

where $\Lambda_{s,i}$ is the de Broglie wavelength of any one nonbonded "segment". The choice of a particular ideal gas reference state defines a corresponding residual Helmholtz energy, as

$$F[\rho_k] \equiv F^{\mathrm{id}}[\rho_k] + F^{\mathrm{res}}[\rho_k] \tag{81}$$

$$\equiv F^{\mathrm{ID}}[\rho_k] + F^{\mathrm{RES}}[\rho_k] \tag{82}$$

We aim at a formulation, where the molecular fluid in the ideal gas is considered as a reference ($F^{\mathrm{id}}[\rho_k]$), where the corresponding residual Helmholtz energy reads

$$F^{\mathrm{res}}[\rho_k] = F^{\mathrm{RES}}[\rho_k] + (F^{\mathrm{ID}}[\rho_k] - F^{\mathrm{id}}[\rho_k]) \tag{83}$$

The difference between the ideal gas states is

$$\begin{aligned}\frac{F^{\mathrm{ID}}[\rho_k] - F^{\mathrm{id}}[\rho_k]}{kT} &= \sum_i (m_i - 1) \int \rho_i(\mathbf{r})\{\ln(\rho_i(\mathbf{r})) - 1\}\mathrm{d}\mathbf{r} \\ &\quad + \sum_i N_i[m_i \ln \Lambda_{s,i}^3 - \ln \Lambda_i^3]\end{aligned} \tag{84}$$

with N_i as the number of molecules i in the system. This difference quantifies the difference of ideal gas molecules to nonbonded ideal gas "segments" for homonuclear chains. We consider the difference in the chain term

$$F^{\mathrm{chain}}[\rho_k] = F^{\mathrm{CHAIN}}[\rho_k] + (F^{\mathrm{ID}}[\rho_k] - F^{\mathrm{id}}[\rho_k]) \tag{85}$$

where F^{CHAIN} is the functional presented by Tripathi and Chapman[46] for homonuclear chains. There, Wertheim's theory accounts for the connectivity of segments to chain (even for ideal gas states). We omit the second term on the right-hand side of eq 84. This term eliminates for all applications because only differences or gradients of the Helmholtz energy are required. eq 85, omitting the second term, leads to eq 14.

■ ASSOCIATED CONTENT

Ⓢ Supporting Information

The Supporting Information is available free of charge on the ACS Publications website at DOI: 10.1021/acs.iecr.6b04551.

Supplementary Tables summarize PCP-SAFT parameters used in this work (PDF)

■ AUTHOR INFORMATION

Corresponding Author

*J. Gross. E-mail: gross@itt.uni-stuttgart.de. Phone: +49 (0) 711 685 66109; +49 (0)711 685 66105. Fax: +49 (0)711 685 66140.

ORCID

Joachim Gross: 0000-0001-8632-357X

Notes

The authors declare no competing financial interest.

■ ACKNOWLEDGMENTS

Financial support of the German Research Council (Deutsche Forschungsgemeinschaft - DFG) through the International Research Training Group "Nonlinearities and upscaling in porous media" (GRK 1398) is gratefully acknowledged.

■ REFERENCES

(1) Evans, R. The nature of the liquid-vapour interface and other topics in the statistical mechanics of non-uniform, classical fluids. *Adv. Phys.* **1979**, *28*, 143−200.

(2) Davis, H. T. *Statistical Mechanics of Phases, Interfaces, and Thin Films*; Wiley-VCH, 1996.

(3) Löwen, H. Density functional theory of inhomogeneous classical fluids: recent developments and new perspectives. *J. Phys.: Condens. Matter* **2002**, *14*, 11897.

(4) Wu, J. Density functional theory for chemical engineering: From capillarity to soft materials. *AIChE J.* **2006**, *52*, 1169−1193.

(5) Vanderlick, T.; Scriven, L.; Davis, H. Molecular theories of confined fluids. *J. Chem. Phys.* **1989**, *90*, 2422−2436.

(6) Evans, R. *Fundamentals of inhomogeneous fluids*; Henderson, D., Ed.; Marcel Dekker, 1992; pp 85−175.

(7) Wu, J.; Li, Z. Density-functional theory for complex fluids. *Annu. Rev. Phys. Chem.* **2007**, *58*, 85−112.

(8) Emborsky, C. P.; Feng, Z.; Cox, K. R.; Chapman, W. G. Recent advances in classical density functional theory for associating and polyatomic molecules. *Fluid Phase Equilib.* **2011**, *306*, 15−30.

(9) Tang, Y.; Wu, J. Modeling inhomogeneous van der Waals fluids using an analytical direct correlation function. *Phys. Rev. E* **2004**, *70*, 011201.

(10) Wertheim, M. Fluids with highly directional attractive forces. I. Statistical thermodynamics. *J. Stat. Phys.* **1984**, *35*, 19−34.

(11) Wertheim, M. Fluids with highly directional attractive forces. II. Thermodynamic perturbation theory and integral equations. *J. Stat. Phys.* **1984**, *35*, 35−47.

(12) Wertheim, M. Fluids with highly directional attractive forces. III. Multiple attraction sites. *J. Stat. Phys.* **1986**, *42*, 459−476.

(13) Wertheim, M. Fluids with highly directional attractive forces. IV. Equilibrium polymerization. *J. Stat. Phys.* **1986**, *42*, 477−492.

(14) Jackson, G.; Chapman, W. G.; Gubbins, K. E. Phase equilibria of associating fluids: Spherical molecules with multiple bonding sites. *Mol. Phys.* **1988**, *65*, 1−31.

(15) Chapman, W. G.; Jackson, G.; Gubbins, K. E. Phase equilibria of associating fluids: Chain molecules with multiple bonding sites. *Mol. Phys.* **1988**, *65*, 1057−1079.

(16) Chapman, W. G.; Gubbins, K. E.; Jackson, G.; Radosz, M. SAFT: Equation-of-state solution model for associating fluids. *Fluid Phase Equilib.* **1989**, *52*, 31−38.

(17) Chapman, W. G.; Gubbins, K. E.; Jackson, G.; Radosz, M. New reference equation of state for associating liquids. *Ind. Eng. Chem. Res.* **1990**, *29*, 1709−1721.

(18) Blas, F. J.; Vega, L. F. Thermodynamic behaviour of homonuclear and heteronuclear Lennard-Jones chains with association sites from simulation and theory. *Mol. Phys.* **1997**, *92*, 135−150.

(19) Blas, F. J.; Vega, L. F. Prediction of binary and ternary diagrams using the statistical associating fluid theory (SAFT) equation of state. *Ind. Eng. Chem. Res.* **1998**, *37*, 660−674.

(20) Gil-Villegas, A.; Galindo, A.; Whitehead, P. J.; Mills, S. J.; Jackson, G.; Burgess, A. N. Statistical associating fluid theory for chain molecules with attractive potentials of variable range. *J. Chem. Phys.* **1997**, *106*, 4168−4186.

(21) Galindo, A.; Davies, L. A.; Gil-Villegas, A.; Jackson, G. The thermodynamics of mixtures and the corresponding mixing rules in the SAFT-VR approach for potentials of variable range. *Mol. Phys.* **1998**, *93*, 241−252.

(22) Gross, J.; Sadowski, G. Application of perturbation theory to a hard-chain reference fluid: an equation of state for square-well chains. *Fluid Phase Equilib.* **2000**, *168*, 183−199.

(23) Gross, J.; Sadowski, G. Perturbed-Chain SAFT: An Equation of State Based on a Perturbation Theory for Chain Molecules. *Ind. Eng. Chem. Res.* **2001**, *40*, 1244−1260.

(24) Lymperiadis, A.; Adjiman, C. S.; Galindo, A.; Jackson, G. A group contribution method for associating chain molecules based on the statistical associating fluid theory (SAFT-γ). *J. Chem. Phys.* **2007**, *127*, 234903.

(25) Papaioannou, V.; Lafitte, T.; Avendaño, C.; Adjiman, C. S.; Jackson, G.; Müller, E. A.; Galindo, A. Group contribution methodology based on the statistical associating fluid theory for heteronuclear molecules formed from Mie segments. *J. Chem. Phys.* **2014**, *140*, 054107.

(26) Müller, E. A.; Gubbins, K. E. Molecular-based equations of state for associating fluids: A review of SAFT and related approaches. *Ind. Eng. Chem. Res.* **2001**, *40*, 2193−2211.

(27) Economou, I. G. Statistical associating fluid theory: A successful model for the calculation of thermodynamic and phase equilibrium properties of complex fluid mixtures. *Ind. Eng. Chem. Res.* **2002**, *41*, 953−962.

(28) Paricaud, P.; Galindo, A.; Jackson, G. Recent advances in the use of the SAFT approach in describing electrolytes, interfaces, liquid crystals and polymers. *Fluid Phase Equilib.* **2002**, *194*, 87−96.

(29) Tan, S. P.; Adidharma, H.; Radosz, M. Recent advances and applications of statistical associating fluid theory. *Ind. Eng. Chem. Res.* **2008**, *47*, 8063−8082.

(30) Zmpitas, W.; Gross, J. Detailed pedagogical review and analysis ofWertheimas thermodynamic perturbation theory. *Fluid Phase Equilib.* **2016**, *428*, 121−152.

(31) Kierlik, E.; Rosinberg, M. A perturbation density-functional theory for polyatomic fluids. I. Rigid molecules. *J. Chem. Phys.* **1992**, *97*, 9222−9239.

(32) Kierlik, E.; Rosinberg, M. A perturbation density functional theory for polyatomic fluids. II. Flexible molecules. *J. Chem. Phys.* **1993**, *99*, 3950−3965.

(33) Kierlik, E.; Rosinberg, M. Perturbation density functional theory for polyatomic fluids. III. Application to hard chain molecules in slitlike pores. *J. Chem. Phys.* **1994**, *100*, 1716−1730.

(34) Segura, C. J.; Chapman, W. G. Associating fluids with four bonding sites against solid surfaces: Monte Carlo simulations. *Mol. Phys.* **1995**, *86*, 415−442.

(35) Segura, C. J.; Chapman, W. G.; Shukla, K. P. Associating fluids with four bonding sites against a hard wall: density functional theory. *Mol. Phys.* **1997**, *90*, 759−772.

(36) Tarazona, P. Free-energy density functional for hard spheres. *Phys. Rev. A: At., Mol., Opt. Phys.* **1985**, *31*, 2672.

(37) Tripathi, S.; Chapman, W. G. Density-functional theory for polar fluids at functionalized surfaces. I. Fluid-wall association. *J. Chem. Phys.* **2003**, *119*, 12611−12620.

(38) Rosenfeld, Y. Free-energy model for the inhomogeneous hard-sphere fluid mixture and density-functional theory of freezing. *Phys. Rev. Lett.* **1989**, *63*, 980.

(39) Roth, R.; Evans, R.; Lang, A.; Kahl, G. Fundamental measure theory for hard-sphere mixtures revisited: the White Bear version. *J. Phys.: Condens. Matter* **2002**, *14*, 12063.

(40) Yu, Y.-X.; Wu, J. Structures of hard-sphere fluids from a modified fundamental-measure theory. *J. Chem. Phys.* **2002**, *117*, 10156−10164.

(41) Yu, Y.-X.; Wu, J. A fundamental-measure theory for inhomogeneous associating fluids. *J. Chem. Phys.* **2002**, *116*, 7094−7103.

(42) Yu, Y.-X.; Wu, J. Density functional theory for inhomogeneous mixtures of polymeric fluids. *J. Chem. Phys.* **2002**, *117*, 2368−2376.

(43) Fu, D.; Wu, J. Vapor-liquid equilibria and interfacial tensions of associating fluids within a density functional theory. *Ind. Eng. Chem. Res.* **2005**, *44*, 1120−1128.

(44) Müller, M.; MacDowell, L.; Yethiraj, A. Short chains at surfaces and interfaces: a quantitative comparison between density-functional theories and Monte Carlo simulations. *J. Chem. Phys.* **2003**, *118*, 2929−2940.

(45) Tripathi, S.; Chapman, W. G. Microstructure and thermodynamics of inhomogeneous polymer blends and solutions. *Phys. Rev. Lett.* **2005**, *94*, 087801.

(46) Tripathi, S.; Chapman, W. G. Microstructure of inhomogeneous polyatomic mixtures from a density functional formalism for atomic mixtures. *J. Chem. Phys.* **2005**, *122*, 094506.

(47) Dominik, A.; Tripathi, S.; Chapman, W. G. Bulk and interfacial properties of polymers from interfacial SAFT density functional theory. *Ind. Eng. Chem. Res.* **2006**, *45*, 6785−6792.

(48) Jain, S.; Dominik, A.; Chapman, W. G. Modified interfacial statistical associating fluid theory: A perturbation density functional theory for inhomogeneous complex fluids. *J. Chem. Phys.* **2007**, *127*, 244904.

(49) Bymaster, A.; Chapman, W. G. An i SAFT density functional theory for associating polyatomic molecules. *J. Phys. Chem. B* **2010**, *114*, 12298−12307.

(50) Blas, F. J.; del Río, E. M.; De Miguel, E.; Jackson, G. An examination of the vapour-liquid interface of associating fluids using a SAFT-DFT approach. *Mol. Phys.* **2001**, *99*, 1851−1865.

(51) Gloor, G. J.; Blas, F. J.; del Río, E. M.; de Miguel, E.; Jackson, G. A SAFT-DFT approach for the vapour-liquid interface of associating fluids. *Fluid Phase Equilib.* **2002**, *194*, 521−530.

(52) Gloor, G. J.; Jackson, G.; Blas, F. J.; del Río, E. M.; de Miguel, E. An accurate density functional theory for the vapor-liquid interface of associating chain molecules based on the statistical associating fluid theory for potentials of variable range. *J. Chem. Phys.* **2004**, *121*, 12740−12759.

(53) Gloor, G. J.; Jackson, G.; Blas, F.; Del Río, E. M.; De Miguel, E. Prediction of the vapor-liquid interfacial tension of nonassociating and associating fluids with the SAFT-VR density functional theory. *J. Phys. Chem. C* **2007**, *111*, 15513−15522.

(54) Schindler, B. J.; Mitchell, L. A.; McCabe, C.; Cummings, P. T.; LeVan, M. D. Adsorption of Chain Molecules in Slit-Shaped Pores: Development of a SAFT-FMT-DFT Approach. *J. Phys. Chem. C* **2013**, *117*, 21337−21350.

(55) Mitchell, L. A.; Schindler, B. J.; Das, G.; dos Ramos, M. C.; McCabe, C.; Cummings, P. T.; LeVan, M. D. Prediction of n-Alkane Adsorption on Activated Carbon Using the SAFT-FMT-DFT Approach. *J. Phys. Chem. C* **2015**, *119*, 1457−1463.

(56) Malheiro, C.; Mendiboure, B.; Plantier, F.; Blas, F. J.; Miqueu, C. Density functional theory for the description of spherical non-associating monomers in confined media using the SAFT-VR equation of state and weighted density approximations. *J. Chem. Phys.* **2014**, *140*, 134707.

(57) Malheiro, C.; Mendiboure, B.; Míguez, J.-M.; Piñeiro, M. M.; Miqueu, C. Nonlocal Density Functional Theory and Grand Canonical Monte Carlo Molecular Simulations of Water Adsorption in Confined Media. *J. Phys. Chem. C* **2014**, *118*, 24905−24914.

(58) Ghobadi, A. F.; Elliott, J. R. Adapting SAFT-γ perturbation theory to site-based molecular dynamics simulation. I. Homogeneous fluids. *J. Chem. Phys.* **2013**, *139*, 234104.

(59) Weeks, J. D.; Chandler, D.; Andersen, H. C. Role of repulsive forces in determining the equilibrium structure of simple liquids. *J. Chem. Phys.* **1971**, *54*, 5237−5247.

(60) Ghobadi, A. F.; Elliott, J. R. Adapting SAFT-γ perturbation theory to site-based molecular dynamics simulation. II. Confined fluids and vapor-liquid interfaces. *J. Chem. Phys.* **2014**, *141*, 024708.

(61) Ghobadi, A. F.; Elliott, J. R. Adapting SAFT-γ perturbation theory to site-based molecular dynamics simulation. III. Molecules with partial charges at bulk phases, confined geometries and interfaces. *J. Chem. Phys.* **2014**, *141*, 094708.

(62) Gross, J. A density functional theory for vapor-liquid interfaces using the PCP-SAFT equation of state. *J. Chem. Phys.* **2009**, *131*, 204705.

(63) Klink, C.; Gross, J. A density functional theory for vapor-liquid interfaces of mixtures using the perturbed-chain polar statistical associating fluid theory equation of state. *Ind. Eng. Chem. Res.* **2014**, *53*, 6169−6178.

(64) Klink, C.; Planková, B.; Gross, J. Density Functional Theory for Liquid-Liquid Interfaces of Mixtures Using the Perturbed-Chain Polar Statistical Associating Fluid Theory Equation of State. *Ind. Eng. Chem. Res.* **2015**, *54*, 4633−4642.

(65) Tang, X.; Gross, J. Density functional theory for calculating surface tensions with a simple renormalization formalism for the critical point. *J. Supercrit. Fluids* **2010**, *55*, 735−742.

(66) von Müller, A.; Leonhard, K. Surface tension calculations by means of a PCP-SAFT-DFT formalism using equation of state parameters from quantum mechanics. *Fluid Phase Equilib.* **2013**, *356*, 96−101.

(67) Shen, G.; Ji, X.; Lu, X. A hybrid perturbed-chain SAFT density functional theory for representing fluid behavior in nanopores. *J. Chem. Phys.* **2013**, *138*, 224706.

(68) Ye, Z.; Cai, J.; Liu, H.; Hu, Y. Density and chain conformation profiles of square-well chains confined in a slit by density-functional theory. *J. Chem. Phys.* **2005**, *123*, 194902.

(69) Shen, G.; Ji, X.; Öberg, S.; Lu, X. A hybrid perturbed-chain SAFT density functional theory for representing fluid behavior in nanopores: Mixtures. *J. Chem. Phys.* **2013**, *139*, 194705.

(70) Shen, G.; Lu, X.; Ji, X. Modeling of molecular gas adsorption isotherms on porous materials with hybrid PC-SAFT-DFT. *Fluid Phase Equilib.* **2014**, *382*, 116−126.

(71) Hansen, J.-P.; McDonald, I. R. *Theory of Simple Liquids*; Elsevier, 1990.

(72) Steele, W. A. The physical interaction of gases with crystalline solids: I. Gas-solid energies and properties of isolated adsorbed atoms. *Surf. Sci.* **1973**, *36*, 317−352.

(73) Tan, Z.; Gubbins, K. E. Adsorption in carbon micropores at supercritical temperatures. *J. Phys. Chem.* **1990**, *94*, 6061−6069.

(74) Gross, J.; Sadowski, G. Application of the perturbed-chain SAFT equation of state to associating systems. *Ind. Eng. Chem. Res.* **2002**, *41*, 5510−5515.

(75) Gross, J. An Equation-of-State Contribution for Polar Components: Quadrupolar Molecules. *AIChE J.* **2005**, *51*, 2556−2568.

(76) Gross, J.; Vrabec, J. An Equation-of-State Contribution for Polar Components: Dipolar Molecules. *AIChE J.* **2006**, *52*, 1194−1204.

(77) Vrabec, J.; Gross, J. Vapor-Liquid Equilibria Simulation and an Equation of State Contribution for Dipole-Quadrupole Interactions. *J. Phys. Chem. B* **2008**, *112*, 51−60.

(78) Mansoori, G.; Carnahan, N.; Starling, K.; Leland, T., Jr Equilibrium thermodynamic properties of the mixture of hard spheres. *J. Chem. Phys.* **1971**, *54*, 1523−1525.

(79) Sauer, E.; Stavrou, M.; Gross, J. Comparison between a homo- and a heterosegmented group contribution approach based on the perturbed-chain polar statistical associating fluid theory equation of state. *Ind. Eng. Chem. Res.* **2014**, *53*, 14854−14864.

(80) Tarazona, P. A density functional theory of melting. *Mol. Phys.* **1984**, *52*, 81−96.

(81) Tarazona, P.; Evans, R. A simple density functional theory for inhomogeneous liquids: Wetting by gas at a solid-liquid interface. *Mol. Phys.* **1984**, *52*, 847−857.

(82) Meister, T.; Kroll, D. Density-functional theory for inhomogeneous fluids: application to wetting. *Phys. Rev. A: At., Mol., Opt. Phys.* **1985**, *31*, 4055.

(83) Curtin, W.; Ashcroft, N. Weighted-density-functional theory of inhomogeneous liquids and the freezing transition. *Phys. Rev. A: At., Mol., Opt. Phys.* **1985**, *32*, 2909.

(84) Peng, B.; Yu, Y.-X. A density functional theory with a mean-field weight function: applications to surface tension, adsorption, and phase transition of a Lennard-Jones fluid in a slit-like pore. *J. Phys. Chem. B* **2008**, *112*, 15407−15416.

(85) Peng, B.; Yu, Y.-X. A density functional theory for Lennard-Jones fluids in cylindrical pores and its applications to adsorption of nitrogen on MCM-41 materials. *Langmuir* **2008**, *24*, 12431−12439.

(86) Rowley, R. L.; Wilding, W. V.; Oscarson, J. L.; Yang, Y.; Zundel, N. A.; Daubert, T. E.; Danner, R. P. *DIPPR Data Compilation of Pure Chemical Properties*; Design Institute for Physical Properties, AIChE, 2009.

(87) Roth, R. Fundamental measure theory for hard-sphere mixtures: a review. *J. Phys.: Condens. Matter* **2010**, *22*, 063102.

(88) Forte, E.; Haslam, A. J.; Jackson, G.; Müller, E. A. Effective coarse-grained solid-fluid potentials and their application to model adsorption of fluids on heterogeneous surfaces. *Phys. Chem. Chem. Phys.* **2014**, *16*, 19165−19180.

(89) Johnson, J. K.; Zollweg, J. A.; Gubbins, K. E. The Lennard-Jones equation of state revisited. *Mol. Phys.* **1993**, *78*, 591−618.

(90) Sokolowski, S.; Fischer, J. Lennard-Jones mixtures in slit-like pores: a comparison of simulation and density-functional theory. *Mol. Phys.* **1990**, *71*, 393−412.

(91) Hemmen, A.; Gross, J. Transferable Anisotropic United-Atom Force Field Based on the Mie Potential for Phase Equilibrium Calculations: n-Alkanes and n-Olefins. *J. Phys. Chem. B* **2015**, *119*, 11695−11707.

(92) Kierlik, E.; Monson, P.; Rosinberg, M.; Sarkisov, L.; Tarjus, G. Capillary condensation in disordered porous materials: Hysteresis versus equilibrium behavior. *Phys. Rev. Lett.* **2001**, *87*, 055701.

(93) Winkler, C.; Maass, O. An investigation of the surface tension of liquids near the critical temperature. *Can. J. Res.* **1933**, *9*, 65−79.

(94) Wu, J.; Liu, Z.; Wang, F.; Ren, C. Surface tension of dimethyl ether from (213 to 368) K. *J. Chem. Eng. Data* **2003**, *48*, 1571−1573.

(95) Jaeger, F. The Dependence on the Temperature of the Molecular Free Surface Energy of Liquids in the Temperature Range −80 to +1650. *Z. Anorg. Allg. Chem.* **1917**, *101*, 214.

(96) Tonomura, T. Measurements of some physical constants of organic compounds at low temperatures. *Sci. Rep. Res. Tohoku A* **1933**, *22*, 104−130.

(97) Bi, S.; Zhao, G.; Wu, J. Surface tension of diethyl ether, diisopropyl ether, and dibutyl ether. *J. Chem. Eng. Data* **2010**, *55*, 1523−1526.

(98) Muratov, G. Surface-tension of benzene and ethyl-alcohol. *Zh. Fiz. Khim.* **1980**, *54*, 2088−2089.

(99) Sprow, F.; Prausnitz, J. Surface tensions of simple liquid mixtures. *Trans. Faraday Soc.* **1966**, *62*, 1105−1111.

(100) Piñeiro, Á.; Brocos, P.; Amigo, A.; Pintos, M.; Bravo, R. Surface tensions and refractive indices of (tetrahydrofuran + n-alkanes) at T = 298.15 K. *J. Chem. Thermodyn.* **1999**, *31*, 931−942.

(101) Schmidt, R. L.; Clever, H. L. Thermodynamics of liquid surfaces: Adsorption at the binary hydrocarbon liquid-vapor interface. *J. Colloid Interface Sci.* **1968**, *26*, 19−25.

(102) Tang, X.; Gross, J. Modeling the phase equilibria of hydrogen sulfide and carbon dioxide in mixture with hydrocarbons and water using the PCP-SAFT equation of state. *Fluid Phase Equilib.* **2010**, *293*, 11−21.

(103) Jańczuk, B.; Wójcik, W.; Zdziennicka, A. Determination of the components of the surface tension of some liquids from interfacial liquid-liquid tension measurements. *J. Colloid Interface Sci.* **1993**, *157*, 384−393.

(104) McQuarrie, D. A. *Statistical Mechanics*; University Science Books, 2000.

(105) Schulte, J. B.; Kreitzberg, P. A.; Haglund, C. V.; Roundy, D. Using fundamental measure theory to treat the correlation function of the inhomogeneous hard-sphere fluid. *Phys. Rev. E* **2012**, *86*, No. 061201.

(106) Barker, J. A.; Henderson, D. Perturbation Theory and Equation of State for Fluids: The Square-Well Potential. *J. Chem. Phys.* **1967**, *47*, 2856−2861.

(107) Barker, J. A.; Henderson, D. Perturbation theory and equation of state for fluids. II. A successful theory of liquids. *J. Chem. Phys.* **1967**, *47*, 4714−4721.

(108) Chen, S. S.; Kreglewski, A. Applications of the Augmented van der Waals Theory of Fluids.: I. Pure Fluids. *Berich. Bunsen. Gesell.* **1977**, *81*, 1048−1052.

(109) Vansteenkiste, P.; Van Speybroeck, V.; Marin, G. B.; Waroquier, M. Ab Initio Calculation of Entropy and Heat Capacity of Gas-Phase n-Alkanes Using Internal Rotations. *J. Phys. Chem. A* **2003**, *107*, 3139−3145.